

Alleviative Effect of Isorhamnetin and
Its Derivatives on Nonalcoholic Steatohepatitis

August 2019

Munkhzul GANBOLD

Alleviative Effect of Isorhamnetin and
Its Derivatives on Nonalcoholic Steatohepatitis

A Dissertation Submitted to
the School of the Integrative and Global Majors,
the University of Tsukuba
in Partial Fulfillment of the Requirements
for the Degree of Doctor of Philosophy in Medical Science
(Doctoral Program in Life Science Innovation)

Munkhzul GANBOLD

Abstract

Nonalcoholic steatohepatitis (NASH) is the most severe and progressive form of nonalcoholic fatty liver disease which affects people who do not or little drink alcohol. The pathogenesis is mostly explained by 'Two-hit hypothesis' representing intra-hepatic lipid accumulation due to metabolic syndromes as the 'first hit' and followed by the 'second hit' resulting in increased inflammation and liver injury with fibrosis. A build-up of fat in the liver so-called steatosis is usually considered benign, but it may progress to more severe pathologic condition over the course of several years when it is combined with inflammation, injury, and fibrosis resulting in NASH which can in turn potentially progress to end-stage liver diseases such as cirrhosis and hepatocellular carcinoma. The fact that NASH pathologic features are reversible which are manifested just before irreversible end-stage liver diseases, it emphasizes the importance and urgency of finding a treatment of NASH to prevent patients to progress into advanced disease steps. However, so far, there are still no drugs approved to treat NASH.

On the other hand, flavonoids are polyphenols widely presented in fruits, vegetables, stems, seeds, etc. Flavonoids are shown to have bioactive effects against metabolic diseases in addition to their strong antioxidant activities. Quercetin is widely studied flavonoid with potentials against carcinoma, inflammation, fibrogenesis, and oxidative stress. Isorhamnetin is an immediate metabolite of quercetin, also found in various plant extracts and plant-derived products. It has been shown to prevent oxidative stress in HepG2 cells [1], inhibit lung and breast cancer cell proliferation [2,3], improve

inflammatory bowel disease [4], and repress adipogenesis in 3T3-L1 cells [5]. Research studies in rodents including investigations in our laboratory, reported the antiobesity, antioxidant, and antifibrotic effects of isorhamnetin or plant extracts rich in isorhamnetin [6,7]. Interestingly, bioavailability reports showed that the most part of absorbed quercetin is found in its methylated form – isorhamnetin which is maintained in plasma longer than quercetin. It strongly implies a potential role of isorhamnetin as a main mediator of beneficial effect of quercetin. Structurally, previous comparative analysis revealed that aglycone flavonoids exert more biological activity compared to their glycones.

Thus, firstly we investigated the effect of isorhamnetin on NASH pathologic features in the liver. NASH was induced in C57BL/6 mice and treated with isorhamnetin orally. Liver and serum were isolated from experimental groups for biometrical, biochemical, histological, gene expression, and micro array analysis. Great number of genes mainly involved in lipid metabolism, oxidation reduction process, and fatty acid metabolism were altered following the induction of NASH. The number of altered genes were remarkably decreased by the isorhamnetin treatment. Consistently, genes involved in fatty acid metabolism, steroid biosynthesis, and PPAR signaling pathway were invariably decreased. In addition, isorhamnetin treatment reduced intrahepatic lipid accumulation associated with lower triglycerides content and inhibited *de novo* lipogenic pathway in NASH-induced mice. Liver injury markers in serum were consistently improved when treated with isorhamnetin compared with their non-treated NASH-

induced littermates. Along with the anti-steatosis effect, isorhamnetin reduced fibrogenic marker gene expressions accompanied with the reduced area of collagen deposition on liver sections. In addition, number of apoptotic cells were significantly decreased after the treatment. Analysis in adipose tissue revealed the infiltration of macrophages in NASH-induced mice showing a chronic inflammatory state while the treatment with isorhamnetin alleviated this inflammatory condition in adipose tissue.

We next sought to identify the structure-activity relationship of methyl group by which isorhamnetin differs from quercetin on the development of fibrosis. To test this hypothesis, we synthesized five different mono-methylated derivatives of quercetin namely isorhamnetin, azaleatin, 3-methylquercetin, tamarixetin, rhamnetin. Hepatic fibrosis is initiated primarily by the hepatic stellate cells (HSC). Chronic injury to liver caused by metabolic disorders, alcoholism, viral infections, and NASH can lead to transdifferentiation of HSCs from its quiescent resting state into its activated state characterized by more migratory, proliferative, and contractile myofibroblast-like phenotype. The activated HSCs promotes extracellular matrix (ECM) molecules including different types of collagens leading to development of fibrosis, and further hepatic injuries which are irreversible. Thus, we used HSCs as an *in vitro* fibrosis model. Fibrosis was induced by transforming growth factor- β (TGF β) in rat stellate cells (HSC-T6), and then cells were treated with methylated derivatives at various dose and time. Immunofluorescence staining of collagen type I (Col1) and alpha smooth muscle actin (α SMA), cell proliferation assay, and fibrogenic gene expression analysis were conducted.

All derivatives showed antiproliferative effects in dose- and time-dependent manner in HSC-T6 cells. Next, TGF β -induced stellate cell was treated with 20 μ M and 40 μ M of derivatives for 24 hours and isorhamnetin, 3MQ, and RHA reduced the protein level and mRNA expression of *Acta2* (gene encoding α SMA); 3MQ prevented the augmentation of *Colla1* (gene encoding Coll1) in TGF β -induced stellate cells. Each compound had different effects against pathologic features of fibrosis which suggests that hydroxyl position plays an important role in the regulation of anti-fibrotic activity of compound. However, the molecular mechanism underlying their antifibrotic effect remains to be elucidated. Our data demonstrated for the first time that methylation could improve the antifibrotic effect of quercetin.

In conclusion, these findings collectively suggest that isorhamnetin elicits beneficial effect on hallmarks of NASH by improving steatosis, injury, and fibrosis in a novel human like NASH-induced mice. This hepatoprotective effect of isorhamnetin was correlated to the inhibition of *de novo* lipogenic and fibrogenic gene expressions; alleviation of liver triglycerides (TG) content; and diminution of hepatic collagen deposition accompanied with the reduced number of apoptotic hepatocytes. Thus, isorhamnetin can be a novel candidate for the additional compound in NASH drug development. Moreover, the addition of methyl group on functionally important position may enhance the antifibrotic effect of quercetin. Further evidence with human NASH will be required to understand the effect of isorhamnetin on NASH development.

Contents

Abstract	1
Contents	5
List of Figures	9
List of Tables	11
Abbreviations and Acronyms.....	12
List of Publication	14
Chapter 1 General Introduction	15
1.1. Nonalcoholic steatohepatitis (NASH) and the etiology.....	16
1.2. Potential effect of isorhamnetin – natural flavonoid	17
1.3. Lack of suitable animal model versus recently developed NASH model	18
1.4. Purpose and content of the thesis	19
Chapter 2 Effect of Isorhamnetin on Steatosis of Mice with Nonalcoholic Steatohepatitis	25
2.1. Introduction.....	26
2.2. Material and methods	28
2.2.1. Animals	28
2.2.2. Chemicals.....	28
2.2.3. Experimental design and procedure	29
2.2.4. Histological analysis.....	29
2.2.5. Total RNA extraction and microarray analysis of liver.....	30
2.2.6. Gene expression analysis	31
2.2.7. Western blotting.....	31

2.2.8. Quantification of liver triglyceride.....	32
2.2.9. Statistical analysis	32
2.3. Results	33
2.3.1. Isorhamnetin reduced liver weight without affecting body weight in NASH-induced mice	33
2.3.2. Isorhamnetin ameliorated hepatic steatosis and TG content in liver	33
2.3.3. Hepatic gene expression profile in NASH and NASH+ISO groups	34
2.3.4. Changes in lipid metabolic process	35
2.3.5. Isorhamnetin decreased hepatic lipid accumulation by inhibiting <i>de novo</i> lipogenic pathway.....	36
2.4. Discussion	43
Chapter 3 Effect of Isorhamnetin on Fibrosis of Mice with Nonalcoholic Steatohepatitis.....	45
3.1. Introduction	46
3.2. Materials and Methods	48
3.2.1. Animals	48
3.2.2. Chemicals.....	48
3.2.3. Experimental design and procedure	48
3.2.4. Blood biochemical analysis.....	49
3.2.5. Histological analysis.....	49
3.2.6. Apoptosis TUNEL assay	49
3.2.7. Total RNA extraction and microarray analysis of liver.....	49
3.2.8. Gene expression analysis	50
3.2.9. Western blotting.....	50
3.2.10. Statistical analysis.....	51

3.3. Results	52
3.3.1. Isorhamnetin treatment improved histopathologic condition of fibrosis and apoptosis in liver with NASH	52
3.3.2. Changes in oxidation reduction process and activation of HSCs	52
3.3.3. Isorhamnetin prevented liver damage and activation of TGF β -mediated profibrotic gene expression	54
3.3.4. Adipocytes enlarged but less infiltrated macrophages in adipose tissue of NASH-induced mice treated with isorhamnetin	54
3.4. Discussion	60
Chapter 4 Effect of Isorhamnetin and Its Derivatives on Fibrosis in TGF β -Induced Hepatic Stellate Cells	62
4.1. Introduction	63
4.2. Materials and Methods	65
4.2.1. NMR data of methylated quercetin.....	66
4.2.2. Chemicals and reagents	66
4.2.3. Cell line and culture condition	66
4.2.4. Cell proliferation assay.....	67
4.2.5. Immunofluorescence-staining analysis.....	67
4.2.6. Real-time reverse transcription polymerase chain reaction (RT-PCR) analysis.....	68
4.2.7. Statistics.....	68
4.3. Results	68
4.3.1. Optimizing TGF β induction in HSC-T6 for fibrosis <i>in vitro</i> model	68
4.3.2. Antiproliferative effects on HSC-T6 after TGF β induction.....	70
4.3.3. Effect of methylated derivatives on Col1 and α SMA production .	70
4.3.4. Effect of methylated derivatives on pro-fibrotic gene expression	71

4.4. Discussion	73
Chapter 5 General Discussion	83
Endnotes.....	89
Acknowledgments	92
References	93

List of Figures

Figure 1.1. Progression stages of liver disease.....	21
Figure 1.2. Chemical structures of quercetin and isorhamnetin.....	22
Figure 1.3. Experimental plan of NASH-induction and the treatment with isorhamnetin.....	24
Figure 2.1. Synthesis schematic of isorhamnetin from quercetin.....	37
Figure 2.2. Biometrics of NASH-induced mice treated with isorhamnetin.	38
Figure 2.3. Effect of isorhamnetin on steatosis of NASH-induced mouse liver.....	39
Figure 2.4. Hepatic gene expression profile in NASH and NASH+ISO group compared to CTL group.....	40
Figure 2.5. Changes in lipid metabolic process.....	41
Figure 2.6. Effect of isorhamnetin on <i>de novo</i> lipogenesis in NASH-induced mice liver.....	42
Figure 3.1. Effect of isorhamnetin on fibrosis and apoptosis of NASH-induced mouse liver.....	56
Figure 3.2. Changes in oxidation reduction process and activation of HSCs.....	57
Figure 3.3. Effect of isorhamnetin on liver injury and fibrogenic gene expression.....	58
Figure 3.4. Effect of isorhamnetin on adipose tissue and lipid profile in serum.....	59
Figure 4.1. Chemical structure and purity of synthesized compounds.....	76
Figure 4.2. Immunodetection of Collagen I and α SMA in TGF β -induced HSCs.....	77
Figure 4.3. Gene expression of α SMA and Collagen I in TGF β -induced HSCs.....	78

Figure 4.4. Effect of TGF β on proliferation of HSCs.	79
Figure 4.5. Inhibitory effect of compounds on proliferation of HSCs.	80
Figure 4.6. Inhibitory effect of compounds on production of α SMA and Collagen I in TGF β -induced HSCs.	81
Figure 4.7. Inhibitory effect of compounds on pro-fibrotic gene expression in TGF β -induced HSCs.	82

List of Tables

Table 1.1. Diet induced and genetically modified rodent models available for NASH. 23

Abbreviations and Acronyms

3MQ	3-O-methylquercetin
<i>Acaca</i>	Gene encoding Acetyl-CoA Carboxylase Alpha
<i>Acta2</i>	Gene encoding actin, alpha 2, smooth muscle
ALT	Alanine aminotransferase
<i>Apolb</i>	Gene encoding Apolipoprotein B
AST	Aspartate aminotransferase
AZA	Azaleatin
BSA	Bovine serum albumin
CCl ₄	Carbon tetrachloride
Col1	Collagen, type I, alpha 1
<i>Colla1</i>	Gene encoding collagen, type I, alpha 1
DAPI	4',6-Diamidino-2-Phenylindole (double stranded DNA staining)
DMEM	Dulbecco's modified eagle medium
DMSO	Dimethyl sulfoxide
DNL	<i>de novo</i> lipogenesis
ECM	Extracellular matrix
FAS	Fatty acid synthase
<i>Fasn</i>	Gene encoding fatty acid synthase
FBS	Fetal bovine serum
GAPDH	Glyceraldehyde 3-phosphate dehydrogenase
HDL	High-density lipoprotein
HE	Hematoxylin and Eosin
HFD	High fat diet
HSCs	Hepatic stellate cells
HSC-T6	Rat hepatic stellate cell line
ISO	Isorhamnetin
LXR	Liver X receptor
MCD	Methionine choline deficient (diet)
MTT	3-(4,5-dimethylthiazol-2-yl)-2,5-diphenyltetrazolium bromide

NAFLD	Nonalcoholic fatty liver disease
NAS	NAFLD activity score
NASH	Nonalcoholic steatohepatitis
NC	Negative control
NMR	Nuclear magnetic resonance
OD	Optical density
PBS	Phosphate buffered saline
PC	Positive control
QCT	Quercetin
RHA	Rhamnetin
SD	Standard deviation
SDS	Sodium dodecyl sulfate
SEM	Standard error of mean
<i>Srebf1</i>	Gene encoding sterol regulatory element binding transcription factor 1
SREBP1c	Sterol regulatory element binding transcription factor 1
TAM	Tamarixetin
TC	Total cholesterol
TG	Triglycerides
TGF β	Transforming growth factor beta 1
<i>Tgfb1</i>	Gene encoding transforming growth factor beta 1
<i>Timp1</i>	Gene encoding tissue inhibitor of metalloproteinase 1
TIMP1	Tissue inhibitor of metalloproteinase 1
VLDL	Very-low-density lipoprotein
α SMA	Actin, alpha 2, smooth muscle

List of Publication

1. Munkhzul Ganbold, Yohei Owada, Yusuke Ozawa, Yasuhiro Shimamoto, Farhana Ferdousi, Kenichi Tominaga, Yun-Wen Zheng, Nobuhiro Ohkohchi and Hiroko Isoda. Isorhamnetin Alleviates Steatosis and Fibrosis in Mice with Nonalcoholic Steatohepatitis. Sci Rep 9, 16210 (2019) doi:10.1038/s41598-019-52736-y
2. Munkhzul Ganbold, Yasuhiro Shimamoto, Farhana Ferdousi, Kenichi Tominaga and Hiroko Isoda. Antifibrotic effect of methylated quercetin derivatives on TGF β -induced hepatic stellate cells. Biochem Biophys Rep. 20, 100678 (2019) doi:10.1016/j.bbrep.2019.100678

Chapter 1

General Introduction

2.1. Nonalcoholic steatohepatitis (NASH) and the etiology

Nonalcoholic fatty liver disease (NAFLD) is considered as a main driver in development and progression of chronic liver diseases, with its global prevalence of 25% among adult population. Hepatic lipid accumulation exceeding 5% of liver weight in the absence of heavy alcohol consumption defines a condition of NAFLD. NAFLD encompasses histological spectrum of stepwise liver pathologies ranging from a simple lipid accumulation (steatosis) to NASH that leads to an end-stage hepatic disease such as cirrhosis, liver failure, and hepatocellular carcinoma, in which liver transplantation remains the sole clinical indication (Figure 1.1). However, steatosis is considered as a liver metabolic manifestation which is reversible, a small subset of patients progresses to NASH. Although NASH prevalence was estimated between 1.5-6.45% in global population, diagnosis of NASH was counted in around a third of NAFLD patients. Recent meta-analysis has also reported alarmingly the rising proportion of NASH incidences was constant within NAFLD prevalence which increased 2-2.4-fold over a 10-year period. Moreover, metabolic comorbidities are highly correlated with NASH. Previous studies reported that there are 82% of individuals with NASH are obese, 44% have type 2 diabetes, and 71% are hyperlipidemic or dyslipidemia. The rates higher than those observed in NAFLD show that predisposition of metabolic syndrome is likely important in the setting of NASH. While hepatic steatosis is more likely considered as a metabolic manifestation of liver which is reversible, NASH has a higher risk to progress to advanced stages of liver diseases.

NASH is characterized by the histological features of hepatocyte damage, lobular inflammation, and fibrosis in addition to fat infiltration. Hypothesis primarily explained its etiology is called “Two-hit theory” in which the “first hit” usually comes from metabolic complications of obesity, insulin resistance, diabetes mellitus, and metabolic syndrome resulting in steatosis in hepatocytes. Oxidative stress, immune system, inflammation, gut and adipose tissue-derived factors, and genetic background, grouped as “Second hits”, are shown to be implicated in the progression of NASH from NAFLD by inducing liver injury and fibrosis. Simultaneous persistence of more than one metabolic disorder for long term may play pivotal role in natural course of NASH leading subsequent pathologic features. But the signaling pathways and molecular mechanisms responsible for its progression from NAFLD to NASH remains unexplained. This gap in our knowledge considerably limits the drug development against NASH. Hypoglycemic and hypolipidemic agents, and physical exercise are recommended in today’s practice to reduce NASH pathologic features. Although these methods have shown some benefic effects, any drugs have not been approved yet to treat NASH.

2.2. Potential effect of isorhamnetin – natural flavonoid

Natural flavonoids have been shown to possess bioactive effects against metabolic diseases. Isorhamnetin is a natural flavonoid found in plant extracts and plant-derived products as well as an intermediate metabolite of quercetin (Figure 1.2). It was reported to inhibit lung and breast cancer cell proliferation [2,3], prevent HepG2 cells

from oxidative stress [1], improve inflammatory bowel disease [4], and repress adipogenesis in 3T3-L1 cells [5]. Research studies in rodents, including investigations in our laboratory, showed its antiobesity, antioxidant, and antifibrotic effects treated with isorhamnetin or plant extracts rich in isorhamnetin [6,7]. Its aglycone parent – quercetin was already demonstrated to possess anti-fibrotic and hepatoprotective activity [8,9], however, reports on bioavailability of quercetin showed that most absorbed latter are found in its methylated form – isorhamnetin which is maintained in plasma longer than quercetin. Li et al. found that isorhamnetin is absorbed more adequately, and is slowly (almost 10 times) eliminated than quercetin [10]. It strongly implies a potential role of isorhamnetin as a main mediator of beneficial effect of quercetin. Structurally, previous comparative analysis revealed that aglycone flavonoids exert more biological activity compared to their glycones. Several studies showed curative and preventive effects of natural flavonoids against the liver diseases.

1.3. Lack of suitable animal model versus recently developed NASH model

It is worth to mention that a suitable animal model is crucial in the research of drug discovery. Researchers still have been seeking an effective drug but the underlying molecular mechanism responsible for etiology of NASH is not completely elucidated yet. Several diet-induced, and genetically modified rodent models have been proposed to imitate NASH pathologies, but none of them could represent along with all hallmarks present in human NASH (Table 1.1). Nonetheless, neither methionine choline deficient

(MCD) diet-induced NASH mice model nor high fat diet (HFD)-induced NAFLD rodent model could represent full NASH hallmarks if the real pathologic context of human NASH needs to be considered. MCD diet-induced NASH mice model is a commonly used aggressive NASH model, however, this model seems to develop neither peripheral insulin resistance nor obesity [11]. Similarly, HFD-induced NAFLD rodent model could not develop hepatic fibrosis, the most important histological predictor for NASH progression in human. However, a novel rodent NASH model was recently developed in the University of Tsukuba [12], which is able to represent main hallmarks of human-like NASH, including liver steatosis, injury and apoptosis, and fibrosis. Owada et al. reported for the first time a triple treatment combination of HFD + carbon tetrachloride (CCl₄ : 0.1 ml/kg, i.p., four times) + LXR-activator T0901317 (T09 : 2.5 mg/kg, i.p., five times) could render C57BL/6J mouse in NASH-positive condition only within 25 days [12]. Briefly, HFD and T09 were used to induce and exacerbate steatosis and oxidative stress, and liver toxin CCl₄ was used to induce fibrosis by causing liver damage. The fact that the liver of this model shows all histopathologic features accompanied with insulin-resistance and obesity, makes this model reliable for drug effectiveness study. The advantage of fast and efficient induction of NASH led us to consider this model suitable in our study. Thus, in this study, we induced NASH in C57BL/6 mice according to Owada's protocol and treated with isorhamnetin as shown in Figure 1.3.

1.4. Purpose and content of the thesis

Discovering drugs to cure a chronic liver disease of which the etiology has not

been completely explained yet, and of which the number incidents in the worldwide is continuously increasing without any successful drug accepted by Food and Drug Administration (FDA) is been a challenging issue for scientist since several decades. Based on the accumulated evidences of isorhamnetin, and the availability of suitable animal model, we attempted to study the effect of isorhamnetin against NASH pathology using molecular and histological analysis.

In chapter 2, morphologic and histopathologic evaluation of liver from NASH-induced mice with or without isorhamnetin treatment, and steatosis and its related gene expression analysis including micro array results were treated. Fibrosis, liver injury, and inflammatory status known as characteristics of NASH were investigated in the chapter 3. We further analyzed, in chapter 4, other mono-methylated analogues of isorhamnetin derived from quercetin for its potential antifibrotic effect using *in vitro* fibrosis model. All findings were discussed collectively in chapter 5 proposing isorhamnetin as a novel candidate for the consideration of additional compound in NASH drug development.

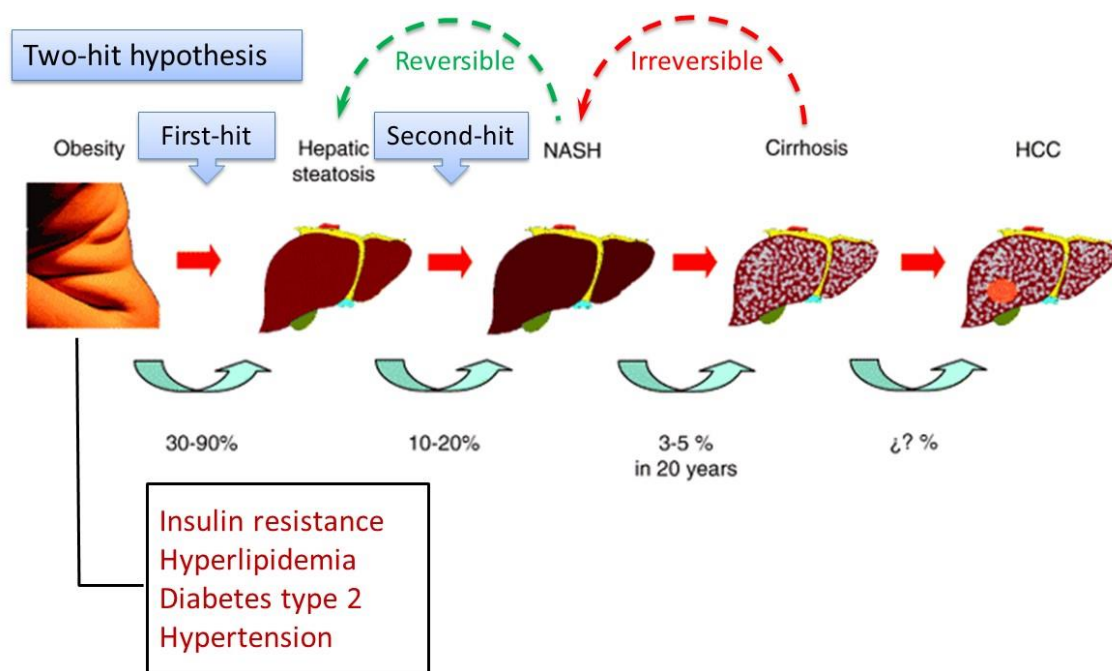


Figure 1.1. Progression stages of liver disease. According to the “two-hit hypothesis” hepatic steatosis is developed in people with metabolic complications, which progress to more severe form NASH distinguished by liver injury, inflammation, and fibrosis. NASH is susceptible to progress to end-stage liver diseases such as cirrhosis and hepatocellular carcinoma. Schematic drawing from Liver Int. 2007 Blackwell Publishing.

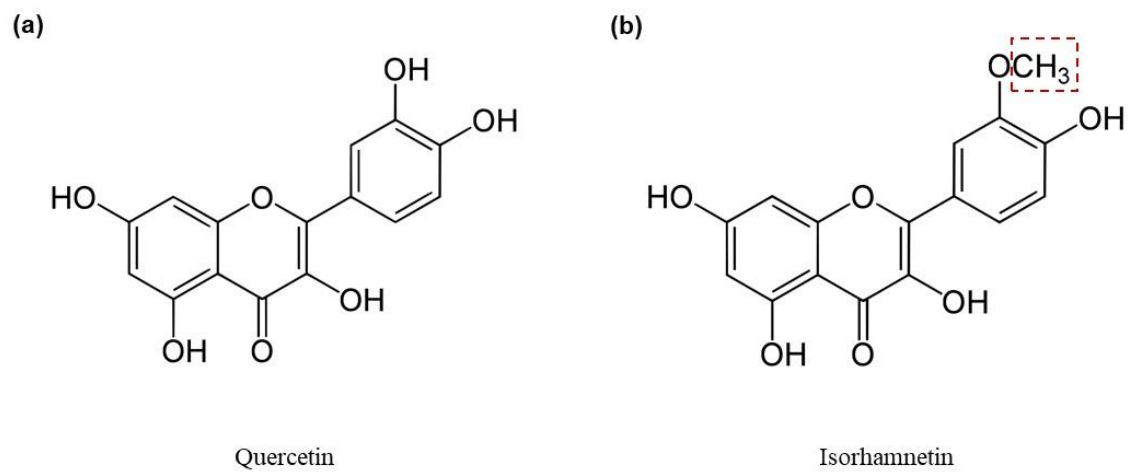


Figure 1.2. Chemical structures of quercetin and isorhamnetin. (a) Quercetin, (b) Isorhamnetin. Red dash line shows the methyl group of isorhamnetin differing from quercetin.

Table 1.1. Diet induced and genetically modified rodent models available for NASH.

	Mice model	Insulin resistance	Steatosis	Steato-hepatitis	Fibrosis	Period
Genetic models	Ob/ob	Yes	Yes	No	No	
	Db/db	Yes	Yes	No	No	
	Fa/fa	Yes	Yes	No	No	
	Agouti	Yes	Yes	No	No	
	MC4R	Yes	Yes	Yes if +HFD	-	1 yr
Dietary models	MCD	No	Yes	Yes	Yes	1-2 wk
	HFD	No	Yes	No	No	10 wk
	WD	Yes	Yes	No	No	6 wk

MCD, methionine choline diet; HFD, high fat diet; WD, western diet; yr, year; wk, weeks.

Groups	Day 0 - 13	Day 14	Day 15	Day 16	Day 17	Day 18	Day 19	Day 20	Day 21	Day 22	Day 23	Day 24	Day 25
CTL	Normal diet												
		Veh			Veh				Veh			Veh	†
								Veh	Veh	Veh	Veh	Veh	
	Veh												
NASH	High Fat Diet												
		CCI4			CCI4				CCI4			CCI4	†
								T09	T09	T09	T09	T09	
	Veh												
NASH+ ISO	High Fat Diet												
		CCI4			CCI4				CCI4			CCI4	†
								T09	T09	T09	T09	T09	
	Isorhamnetin												

Figure 1.3. Experimental plan of NASH-induction and the treatment with isorhamnetin.

NASH was induced within 24 days in C57BL/6 mice subjected to high fat diet, using intraperitoneal injection with CCl₄ (0.1 ml/kg of body weight, 4 times) and T09 (2.5 ml/kg of body weight, 5 times) as indicated. Isorhamnetin was administered 50 mg/kg of body weight during Day 14-24 by oral route. Veh – vehicle, and † - sacrifice.

Chapter 2

Effect of Isorhamnetin on Steatosis of Mice
with Nonalcoholic Steatohepatitis

2.1. Introduction

Metabolic comorbidities are highly correlated with NASH. Previous studies reported that among individuals with NASH 82% are obese, 44% have type 2 diabetes, and 71% are hyperlipidemic or having dyslipidemia [13]. All these metabolic complications contribute to liver lipid accumulation as called hepatic steatosis which is defined by lipid content exceeding 5% of liver weight in the absence of heavy alcohol consumption. However, steatosis alone is considered as a liver metabolic manifestation which is reversible, a small subset of patients with hepatic steatosis progress to NASH associated with increased risk of progression to advanced forms of liver diseases.

Steatosis resulted from different metabolic complications is usually manifested as a “first hit” in the onset of NASH, on which further NASH pathologies are developed. Thus, tackling with steatosis is more likely an indispensable step to prevent and eventually treat NASH. Fatty acids stored in the liver arise from three main sources: around 60% from fat-rich diet, 10-20% from lipolysis of adipose tissue, and 20-30% from hepatic *de novo* lipogenesis (DNL) [14]. In current clinical practice, diet source and lipolysis of adipose tissue can be controlled up to certain extent by managing diet regime combined with pharmacological strategies. In NAFLD and NASH patients, DNL pathway in liver is constantly activated because of insulin resistance and contributes to exacerbation of hepatic steatosis [15–17].

In this chapter, we evaluated the anti-steatosis effect of isorhamnetin in the liver of mice with NASH considering the main contributing pathways of fatty acid influx to

liver, especially hepatic DNL pathway was targeted. We did not take into consideration the dynamics of dietary fatty acid influx within the scope of our study because the mice in NASH and NASH+ISO groups were equivalently subjected to high fat diet regime, and the drastic increase of dietary fatty acid was expected. To this end, we induced NASH in mice and treated them with isorhamnetin by oral gavage and evaluated its biological efficacy in the alleviation of steatosis in NASH model.

2.2. Material and methods

Detailed methodology of experiments was explained in the endnote.

2.2.1. Animals

Six-week-old male C57BL/6J mice (Charles River Laboratories JAPAN Inc., Kanagawa, Japan) were maintained at room temperature in a 12h light/dark cycle. After one week of acclimatization with standard chow diet and tap water *ad libitum*, all animals were randomly assigned (Day 0) into three experimental groups (n = 8/group): Control (CTL), NASH, and NASH treated with isorhamnetin (NASH+ISO). All animal procedures were approved by the Animal Study Committee of University of Tsukuba (No.17-312) and were handled according to the Guiding Principles for the Care and Use of Animals in the Field of Physiological Sciences approved by The Physiological Society of Japan.

2.2.2. Chemicals

Isorhamnetin was synthesized from commercially available quercetin (Fujifilm Wako Pure Chemical Corp., Tokyo, Japan) according to the protocol [18] and used in *in vivo* experiments. Scheme of synthesis of isorhamnetin from quercetin was shown in Fig. 2.1. Commercially available selective agonist for LXR α and LXR β (T0901317) (Cayman Chemical, Ann Arbor, MI, USA); and carbon tetrachloride (CCl₄) (Wako Pure Chemical Industries Ltd., Osaka, Japan) were used.

2.2.3. Experimental design and procedure

NASH was induced according to the protocol [12]. Briefly, the CTL group mice were fed with laboratory chow diet and received vehicles. NASH and NASH+ISO groups were subjected to high fat diet (60% kcal % fat, D12492, Research Diets Inc., New Brunswick, NJ, USA) from Day 0-24. Rodents received intraperitoneal injections of CCl₄ at 0.1ml/kg of body weight 4 times (Day 14, 17, 21, and 24), and T0901317 at 2.5ml/kg of body weight 5 times (Day 20-24) to induce NASH. Corn oil and dimethyl sulfoxide (DMSO) were used as vehicle for CCl₄ and T0901317 injections respectively. NASH+ISO group was treated with daily oral administration of isorhamnetin at 50 mg/kg of body weight (vehicle for CTL and NASH group) for last two weeks (Day 11-24). Body weight and food intake were measured every day. At the end of experiment (Day 25) blood was collected from retro-orbital sinus using capillary tube after mice are slightly anesthetized with isoflurane inhalation. Serum was separated after centrifugation at 3000 rpm for 10 min and was stored at -20°C until biochemical analysis. Liver and epididymal fat were isolated immediately after the exsanguination. Median lobe of liver was stocked in either liquid nitrogen or cryopreserves for further analysis. Remaining liver was fixed in 10% neutral buffered formalin for histological staining.

2.2.4. Histological analysis

Tissues embedded in paraffin were sliced into sections and stained with Hematoxylin and Eosin (HE) using standard protocol for histopathology analysis of liver.

Cryopreserved liver tissues were sliced and used for oil red O staining with hematoxylin counterstaining. Stained slides were observed under a BZ-9000 BioRevo digital microscope (Keyence Corp., Osaka, Japan), and were analyzed using ImageJ.

2.2.5. Total RNA extraction and microarray analysis of liver

The total RNA of liver tissues was extracted using ISOGEN reagent (Nippon Gene Co., Ltd. Toyama, Japan) according to the manufacturer's protocol. The quality and quantification of total RNA was measured on NanoDrop 2000 spectrophotometer (Thermo Scientific, Wilmington, DE, USA), and 100 ng of RNA input was used for microarray analysis. The gene expression profiling was performed using GeneChip 3' IVT PLUS Reagent Kit (Affymetrix Inc., Santa Clara, CA, USA) with Affymetrix® 3' IVT Array Strips for GeneAtlas® System (GeneChip® MG-430 PM) according to the manufacturer's user guide. Raw intensity values were obtained using GeneAtlas™ Imaging Station and normalized using Expression Console Software provided by the Affymetrix following robust multichip average (RMA) algorithm (<http://www.affymetrix.com>). Subsequently, the raw data set was transferred to the Transcriptome Analysis Console (TAC) v4.0 (ThermoFisher inc.). A threshold with fold-change ≥ 2.0 and $p > 0.05$ were considered as differentially expressed genes (DEGs) compared to CTL. Further analyses were conducted using Functional annotation tool of The Database for Annotation, Visualization and Integrated Discovery (DAVID) v6.8 online bioinformatics database to identify enriched Gene ontology (GO) and KEGG

pathways. Heat maps were visualized with DEGs in each biological process identified by GO using Morpheus online tool (<https://software.broadinstitute.org/morpheus>). Box plots analyses were visualized using GraphPad Prism 8 which show the average of genes implicated in each process.

2.2.6. Gene expression analysis

The total RNA of liver tissues was extracted as described in Section 2.2.5. Reference of primers and protocols are detailed in the endnoteⁱ.

2.2.7. Western blotting

Total protein was extracted from liver tissue (50 mg) using radio immunoprecipitation assay (RIPA) buffer (Sigma-Aldrich, St. Louis, USA) containing protease inhibitor cocktail (P8340, Sigma-Aldrich, St. Louis, MO, USA), and quantified with 2-D Quant kit (GE Healthcare, Chicago, USA) following the manufacturer's instruction. Protein samples (20 µg) were resolved in 10% SDS-PAGE and transferred to nitrocellulose membrane. After blocking in Odyssey blocking buffer (LI-COR, NE, USA) for 2 hours, membranes were blotted with primary antibody for overnight at 4 °C and incubated with appropriate Alexa Fluor® conjugated secondary antibodies. Imaging and quantification of signal intensity were detected using Odyssey Fc Imaging System (LI-COR, NE, USA). Primary antibodies: rabbit anti-FAS (ab22759), rabbit anti-SREBP1 (ab28481), mouse anti-GAPDH (ab8245), and secondary antibodies: Alexa Fluor® 488-

conjugated donkey anti-rabbit (ab150073), Alexa Fluor® 594-conjugated donkey anti-mouse (ab150108) were purchased from Abcam.

2.2.8. Quantification of liver triglyceride

Total TG in liver were quantified using commercially available colorimetric kit (Cayman Chemical, Ann Arbor, MI, USA).

2.2.9. Statistical analysis

All data are expressed as the mean \pm SEM. Normality test was performed to confirm the normal distribution. A one-way analysis of variance (ANOVA) followed by Tukey's post hoc test was applied to assess the statistical significance of difference among the treatment groups. A value of $p < 0.05$ was considered as significant for all results. Statistical analyses were performed using IBM SPSS Statistics version 24.0.

2.3. Results

2.3.1. Isorhamnetin reduced liver weight without affecting body weight in NASH-induced mice

In this study, the novel NASH model was induced for its similarity to human NASH including steatosis, lobular inflammation, hepatocellular injury, and fibrosis. Livers of both NASH and NASH+ISO groups were significantly enlarged and pale in color indicating fatty liver aspect compared to those of CTL group which were reddish-brown color and small sized (Figure 2.2.a). Compared to CTL group the other two groups had increased food intake in calories and weight gain, however, no significant difference was observed in daily calorie intake and change in body weight between NASH and NASH+ISO groups (Figure 2.2.b, e). Liver weights of NASH and NASH+ISO groups were indifferent (Figure 2.2.c). In contrast, liver on body weight ratio was significantly reduced in isorhamnetin-treated NASH mice compared to non-treated NASH mice (Figure 2.2.d), suggesting that isorhamnetin decreased liver weight although body weight was not affected.

2.3.2. Isorhamnetin ameliorated hepatic steatosis and TG content in liver

Fatty liver or hepatic steatosis is an indispensable prerequisite of diagnosis in patients with NASH. Liver steatosis was evaluated with HE and oil red O staining, and results are shown in Figure 2.3.a, b. CTL group did not contain any lipid in hepatocytes. NASH-induced liver exhibited severe accumulation of lipids exceeding 37% of oil red O

positive area, whereas isorhamnetin treatment mitigated it until 22% (Figure 2.3.c). Concordant with the ameliorated steatosis, the TG content in liver was also significantly reduced to 76 mg/g of liver weight in NASH+ISO group compared to 99 mg/g in NASH group ($p = 0.029$) (Figure 2.3.d). This finding correlates with the reduced liver to body weight ratio observed in isorhamnetin-treated NASH mice (Figure 2.2.d).

2.3.3. Hepatic gene expression profile in NASH and NASH+ISO groups

To clarify the expression pattern of genes in the liver following the induction of NASH and its changes regulated by isorhamnetin treatment, we have performed a microarray gene expression analysis. Among the 45055 probe sets, number of genes with fold change greater than ± 2.0 and p value threshold of less than 0.05 compared to CTL were considered as differentially expressed genes (DEGs) as shown in volcano plot (Figure 2.4.a). Upregulated number of DEGs in NASH was remarkably reduced in NASH+ISO (Figure 2.4.b). The 404 overlapping genes were found between NASH and NASH+ISO (Figure 2.4.c). In gene ontology (GO) analysis, the upregulated genes resulting from the overlapped genes were greatly associated with lipid metabolism (GO:0006629), oxidation reduction process (GO:0055114), metabolic (GO:0008152) especially fatty acid (GO:0006631) and cholesterol (GO:0008203) metabolic processes (Figure 2.4.d), while downregulated genes were related to oxidation-reduction (GO:0055114), epoxygenase P450 pathway (GO:0019373), and methylation process (GO:0032259) (Figure 2.4.e). Along with the GO process, the upregulated genes were

enriched in the metabolic pathways (mmu01100), biosynthesis of antibiotics (mmu01130), fatty acid metabolism (mmu01212), and PPAR signaling pathway (mmu03320) in Kyoto Encyclopedia of Genes and Genomes (KEGG) analysis (Figure 2.4.d). In addition, metabolic pathway, retinol metabolism (mmu00830), and steroid hormone biosynthesis (mmu00140) pathways enriched by downregulated genes were top-ranked in KEGG pathway (Figure 2.4.e). These data show that isorhamnetin treatment reduced the number of altered gene expressions due to the induction of NASH.

2.3.4. Changes in lipid metabolic process

The substantial number of genes were upregulated in lipid metabolism with the development of NASH as revealed by the GO analysis. Thus, we analyzed the genes (58 genes in total) identified by heat map comparing NASH vs. CTL and NASH+ISO vs. CTL (Figure 2.5.a). Interestingly, the reduced level of expression for 42 genes was found in NASH+ISO compared to NASH. Next, we sought to distinguish genes by pathway axis which are involved in lipid metabolic process. As expected, the essential gene expressions in fatty acid metabolism, steroid biosynthesis, and PPAR signaling pathway were invariably decreased in NASH+ISO, while the median change of gene expression levels in fatty acid degradation was not different between groups although NASH+ISO group genes tend to be decreased (Figure 2.5.b).

2.3.5. Isorhamnetin decreased hepatic lipid accumulation by inhibiting *de novo* lipogenic pathway

To clarify if the anti-steatosis effect of isorhamnetin was due to the inhibition of DNL pathway, we analyzed mRNA expression of key lipogenic genes. SREBP1c is a master regulator of lipogenesis and mediates insulin-induced lipogenic pathway. Other two lipogenic enzymes involved in fatty acid synthesis are FAS and ACC1 that are transcriptionally upregulated by SREBP1c [14,19]. We found that mRNA expression of *Srebf* (gene encoding SREBP1c), *Fasn* (gene encoding FAS), consistent with the corresponding protein level, and *Acaca* (gene encoding ACC1) was significantly upregulated ($p < 0.001$) in NASH-induced liver compared to CTL group, while SREBP1c-mediated DNL pathway was considerably inhibited ($p < 0.001$ for all genes) in NASH+ISO group when compared with NASH group. Decreased level of apolipoprotein B (*Apob*), a rate-determining protein of lipid export in liver, is observed in NASH. The *Apob* gene expression level was significantly reduced in NASH group compared to CTL but the level in NASH+ISO was similar to that of NASH group (Figure 2.6.a, b). These findings collectively show that the substantially altered lipid metabolic process in NASH was efficiently improved, and DNL was in part inhibited by the isorhamnetin treatment.

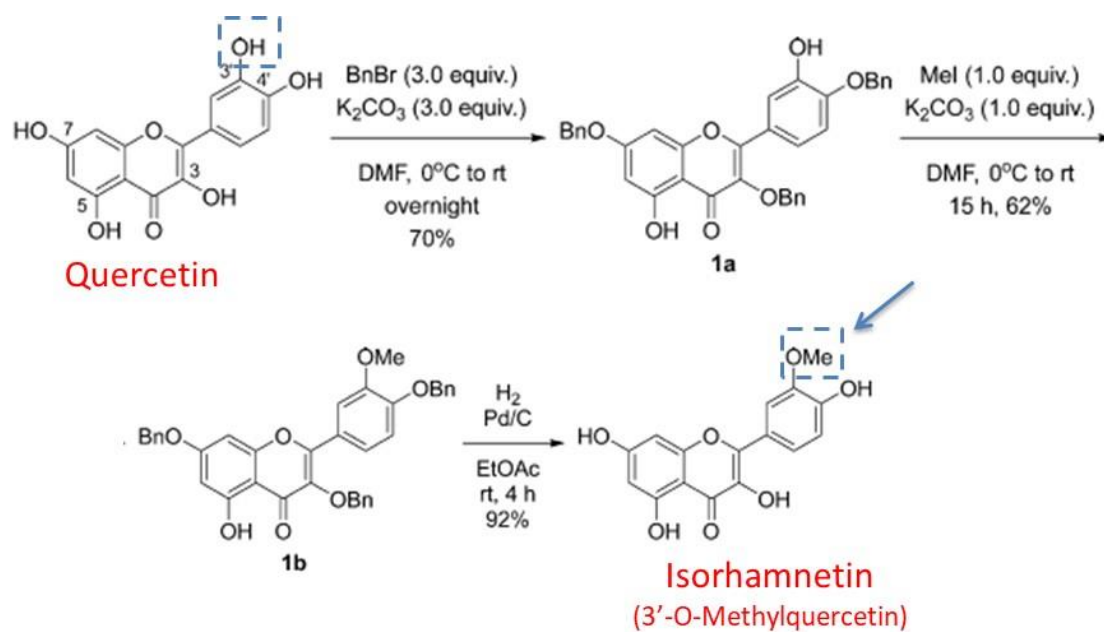


Figure 2.1. Synthesis schematic of isorhamnetin from quercetin. Synthesis of isorhamnetin was carried out in the Interdisciplinary Research Center for Catalytic Chemistry, National Institute of Advanced Industrial Science and Technology (AIST), and provided us for research use.

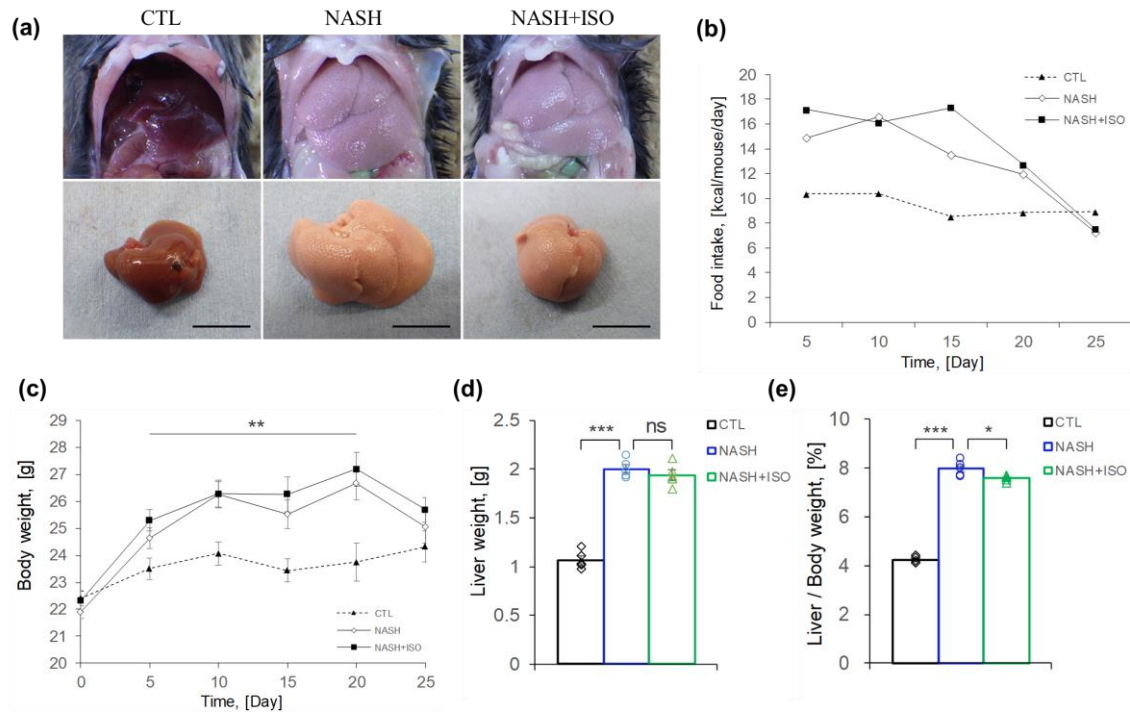


Figure 2.2. Biometrics of NASH-induced mice treated with isorhamnetin. (a) Representative liver aspect of experimental groups: control (CTL), NASH-induced (NASH), and NASH-induced with isorhamnetin treatment (NASH+ISO) group (scale bar = 1 cm). (b) Average food intake in calories of experimental groups presented as kcal per mouse per day (n = 8 / group). (c) Body weight change (n = 8 / group). (d) Effect of isorhamnetin on liver weight (n = 5 / group, NASH vs. NASH+ISO: p = 0.389) and (e) liver on body weight ratio (n = 5 / group, NASH vs. NASH+ISO: p = 0.025). Data are shown as mean \pm SEM with significance *p < 0.05, **p < 0.01, ***p < 0.001 and ns = non-significant.

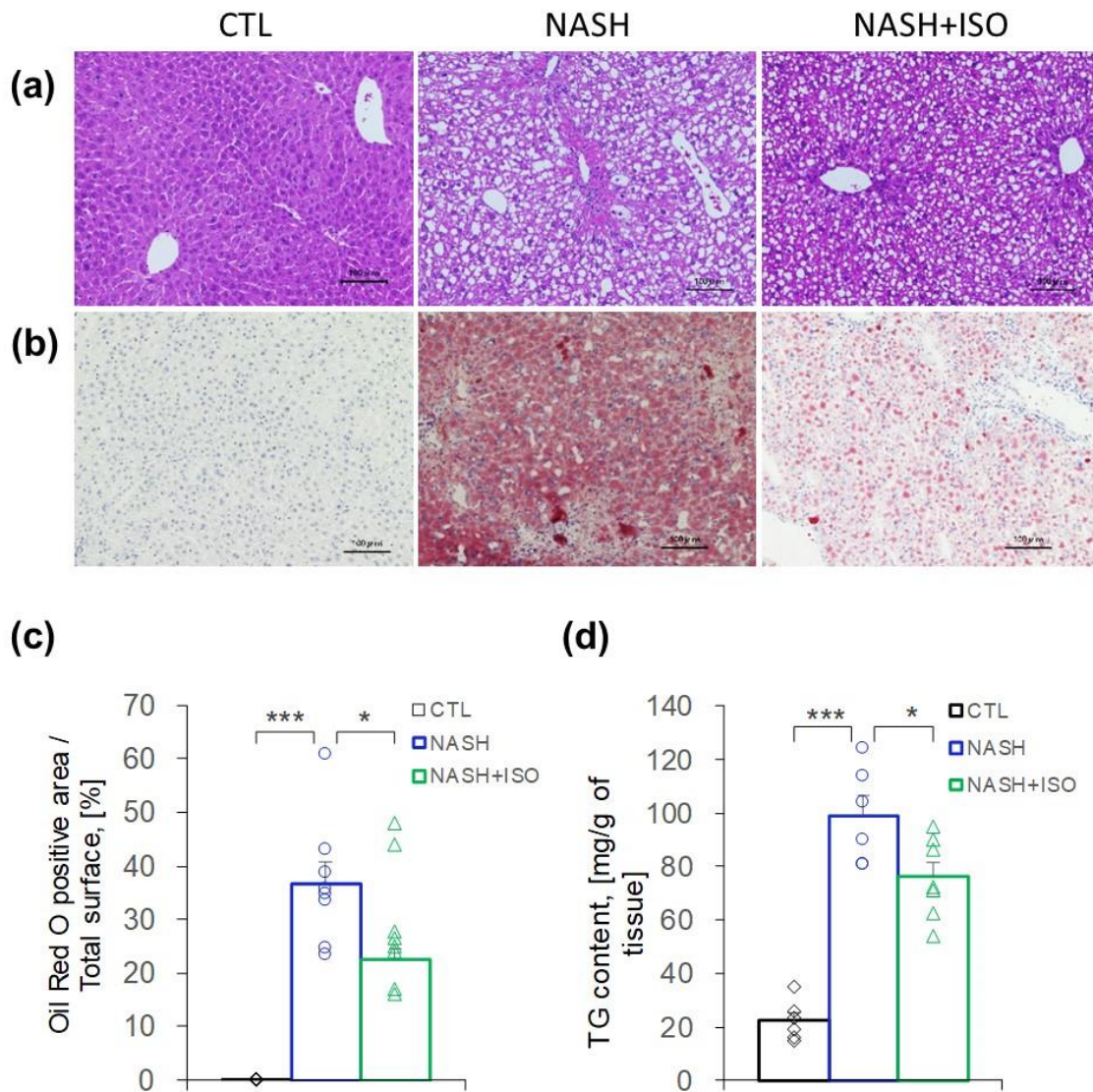


Figure 2.3. Effect of isorhamnetin on steatosis of NASH-induced mouse liver. Representative microscopic images of HE-stained (a), oil red O-stained (b) liver sections (scale bar = 0.1 mm). (c) Quantification of oil red O positive area (n = 8 / group, NASH vs. NASH+ISO group: p = 0.017). (d) Quantification of triglycerides in liver (mg / g of tissue, n = 6 / group in CTL and NASH, n = 7 in NASH+ISO group, NASH vs. NASH+ISO: p = 0.029). Data are shown as mean \pm SEM with significance *p < 0.05, and ***p < 0.001.

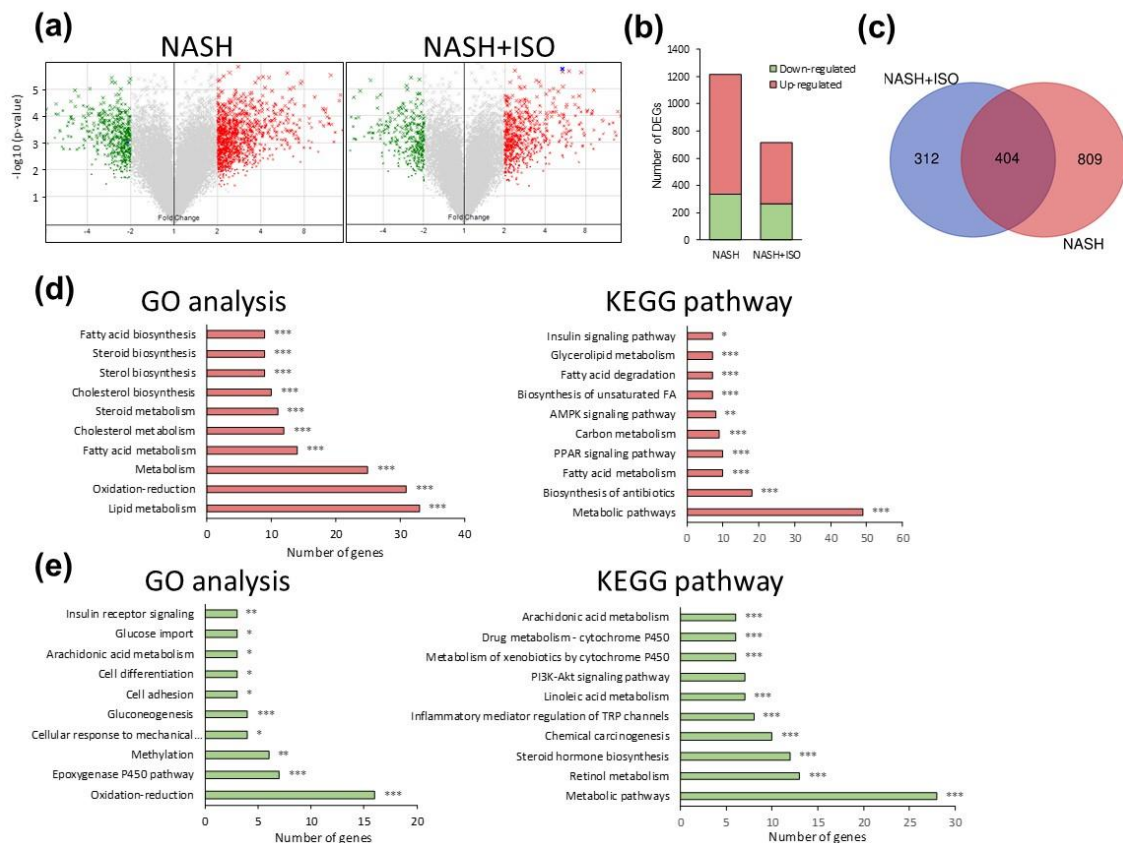


Figure 2.4. Hepatic gene expression profile in NASH and NASH+ISO group compared to CTL group. (a) Volcano plot of DEGs with fold-change over ± 2.0 (green: down-regulated, and red: up-regulated genes) between NASH vs. CTL, and NASH+ISO vs. CTL. (b) Quantitation of number of DEGs. (c) Venn diagram showing the overlap of DEGs between NASH vs. CTL, and NASH+ISO vs. CTL. GO process analysis and KEGG pathway for the up-regulated 257 genes (d) and down-regulated 147 genes (e) from overlapping 404 DEGs with p-value as * $p < 0.05$, ** $p < 0.01$, *** $p < 0.001$.

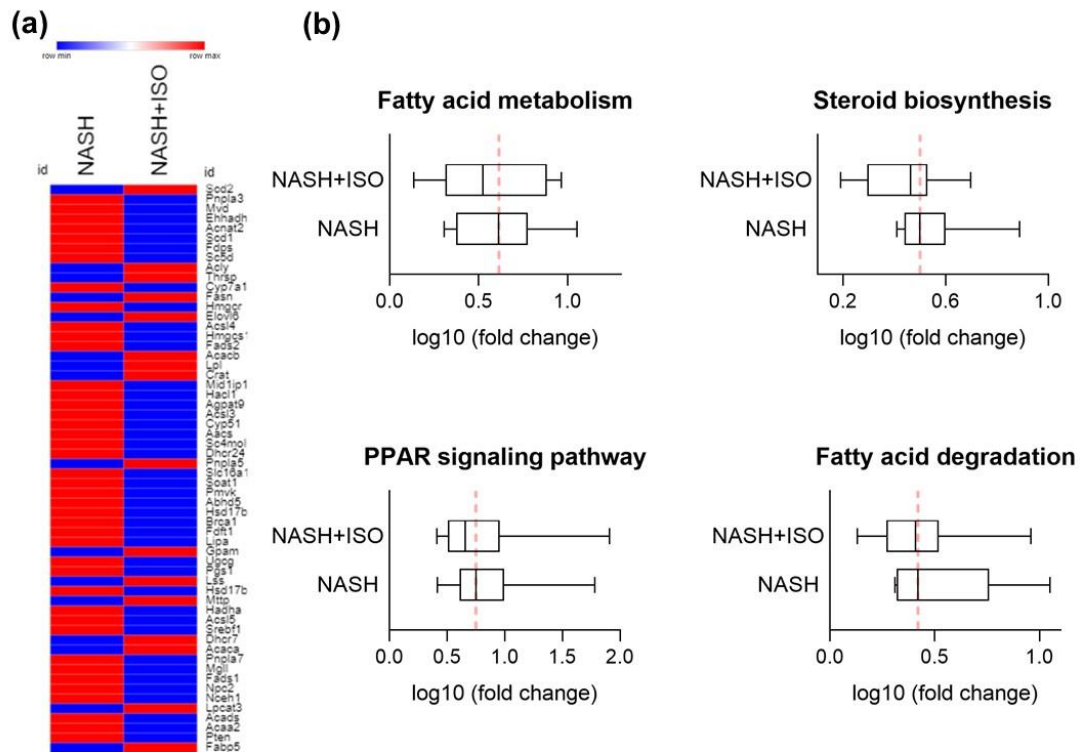


Figure 2.5. Changes in lipid metabolic process. (a) Heat map showing DEGs involved in lipid metabolic pathways between NASH and NASH+ISO compared to CTL group. (b) Box plot with median averaging genes involved in fatty acid metabolism (13 genes averaged), steroid biosynthesis (9 genes averaged), PPAR signaling pathway (10 genes averaged), and fatty acid degradation (7 genes averaged). Red dash line shows the median of NASH group.

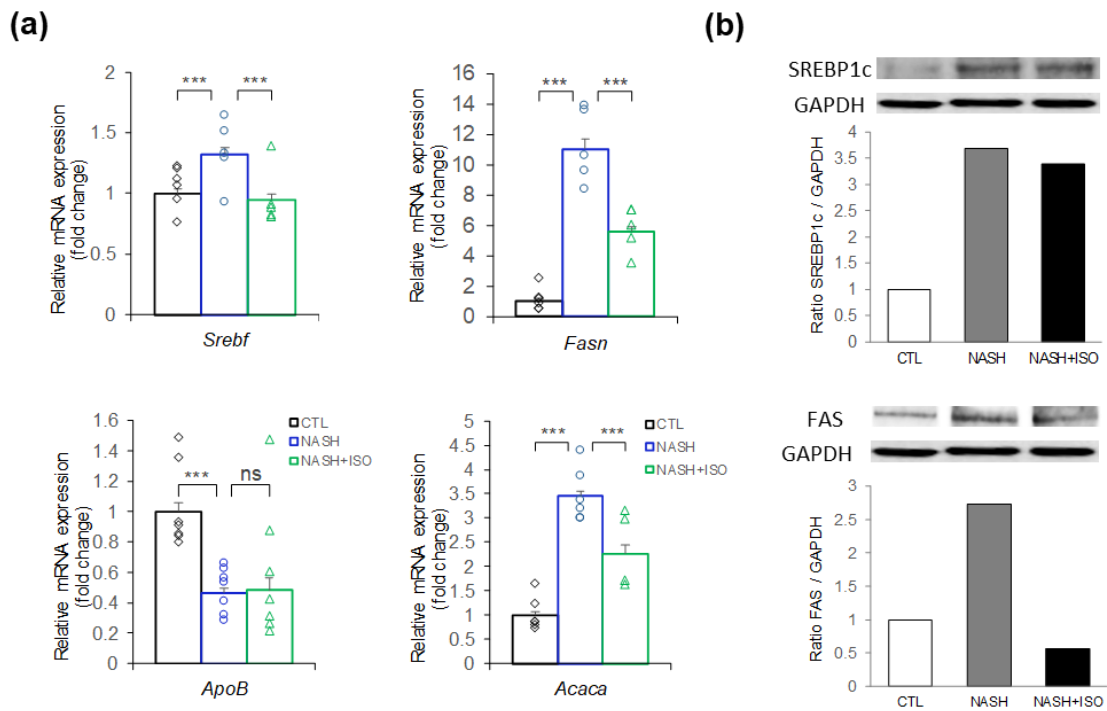


Figure 2.6. Effect of isorhamnetin on *de novo* lipogenesis in NASH-induced mice liver. (a) Relative mRNA expression level of *de novo* lipogenic and lipid transportation genes (n = 4-6 / group) by qPCR analysis. Data are shown as mean \pm SEM with significance ***p < 0.001. (b) Immunoblot analysis for SREBP1c and Fatty acid synthase (FAS) in liver tissue and quantification of band intensities normalized to GAPDH.

2.4. Discussion

Lipid accumulation in liver is been suggested to manifest in prior to the setting of NASH and may come from three main sources: around 60% from fat-rich diet, 10-20% from lipolysis of adipose tissue, and 20-30% from hepatic DNL [14]. Obesity, and insulin resistance are all considered to as risk factors for development of NASH. Our NASH-induced mice model represents insulin resistance, and hyperglycemia [12]. In addition, NASH-induced mice had enlarged steatotic liver compared to CTL. Furthermore, histologic findings showed important infiltration of lipid in hepatocytes supported by the increased content of TG in NASH group. Isorhamnetin treatment greatly improved steatotic condition and the ratio of liver weight to body weight.

Micro array analysis was performed to clarify the molecular pathways which might be affected following the induction of NASH and the treatment with isorhamnetin. Highest number of genes implicated in metabolic process especially in fatty acid and cholesterol metabolism, and redox process were significantly expressed in NASH. The total number of upregulated genes, and median fold-change of genes grouped by their lipid metabolic process were consistently decreased in NASH+ISO, indicating that isorhamnetin prevented the chronic steatosis caused by highly altered metabolic genes expression in NASH.

Moreover, we analyzed the expression of key genes involved in DNL and found that isorhamnetin treatment of NASH-induced mice could attenuate DNL pathway by regulating lipogenic key transcription factor, SREBP1c, which, in turn, downregulated

lipogenic enzymes. This result correlates with the histological findings of reduced hepatic TG content and intrahepatic lipid accumulation in isorhamnetin-treated NASH mice compared to untreated NASH mice.

ApoB is a protein synthesized in liver and is required for the formation of very low-density lipoprotein (VLDL). The VLDL exports liver TG from liver and delivers to body tissues, including adipose tissue. Previous studies demonstrated that hepatic ApoB production is decreased in NASH patients resulting in diminished secretion of VLDL and increased hepatic steatosis [20]. Thus, we compared mRNA expression level of *Apob* among all three groups. In NASH-induced groups the expression of *Apob* was attenuated significantly compared to that of in CTL group and isorhamnetin treatment did not rescue this alteration.

Based on these results, we further sought to analyze fibrotic and injured condition of liver with NASH and the effect of isorhamnetin treatment on these pathologic features in the following Chapter 3, because liver steatosis, inflammation, and fibrosis are interrelated, and are likely to aggravate each other by positive feedback leading to progression of NASH.

Chapter 3

Effect of Isorhamnetin on Fibrosis of Mice with Nonalcoholic Steatohepatitis

3.1. Introduction

Following the findings in Chapter 2, isorhamnetin showed anti-steatosis effect in NASH-induced liver. We also sought to evaluate, in this chapter, the fibrosis, liver injury, and apoptotic status in the liver with NASH which are considered characteristics of NASH. Liver fibrosis is characterized by excessive accumulation of extracellular matrix (ECM) leading to irreversible damage and advanced stages of hepatic diseases if the injury is persistent and chronic.

ECM contains abundant collagen protein and plays an essential role in temporary protection of tissues from incurring injuries allowing cells to regenerate [21]. However, repeated chronic injuries can alter ECM remodeling, eventually leading to the scar formation resulting in hepatic fibrosis. Thus, we assessed the effect of isorhamnetin on the development of fibrosis. TGF β is the principal profibrotic cytokine, which is increased in response to hepatic insults and inflammation through activation of HSCs. TGF β is known to mediate hepatic fibrosis by activating HSCs which result in increased ECM production [22].

Alanine aminotransferase (ALT) and aspartate aminotransferase (AST), is immediately increased when hepatocytes are subjected to acute injury. Thus, the serum level of these enzymes is the primary tool to evaluate liver injury state. During the development of NASH, increased oxidative stress causes the damage in liver which results in apoptosis of hepatocytes. Along with the excessive production of ECM, the increased number of apoptotic cells aggravate the physiologic regulation of liver leading

to the fibrogenesis. NASH with fibrosis is the most severe form of nonalcoholic diseases, considered as pre-cirrhosis condition.

In addition, research studies including investigations in our laboratory showed strong antiobesity, antioxidant, and antifibrotic effects in rodents treated with isorhamnetin or plant extracts rich in isorhamnetin [6,7,23]. Thus, in this chapter we performed micro array analysis, histopathologic evaluation, gene expression and protein level measurement by western blotting to clarify the potential effect of isorhamnetin treatment against fibrosis-related features in liver of NASH-induced mice.

3.2. Materials and Methods

3.2.1. Animals

Six-week-old male C57BL/6J mice (Charles River Laboratories JAPAN Inc., Kanagawa, Japan) were maintained at room temperature in a 12 h light/dark cycle. After one week of acclimatization with standard chow diet and tap water *ad libitum*, all animals were randomly assigned (Day 0) into three experimental groups (n = 8/group): Control (CTL), NASH, and NASH treated with isorhamnetin (NASH+ISO). All animal procedures were approved by the Animal Study Committee of University of Tsukuba (No.17-312) and were handled according to the Guiding Principles for the Care and Use of Animals in the Field of Physiological Sciences approved by The Physiological Society of Japan.

3.2.2. Chemicals

Isorhamnetin was synthesized from commercially available quercetin (Fujifilm Wako Pure Chemical Corp., Tokyo, Japan) according to the protocol [18] and used for *in vivo* experiment. Commercially available selective agonist for LXR α and LXR β (T0901317) (Cayman Chemical, Ann Arbor, MI, USA); and carbon tetrachloride (CCl₄) (Wako Pure Chemical Industries Ltd., Osaka, Japan) were used.

3.2.3. Experimental design and procedure

Experimental design and procedure was mentioned in the section 2.2.3.

3.2.4. Blood biochemical analysis

The total cholesterol (TC), TG, high-density lipoprotein (HDL), ALT, AST levels in serum were measured using FUJI DRI-CHEM 7000 automated chemistry analyzer (Fujifilm Corp. Tokyo, Japan).

3.2.5. Histological analysis

Tissues embedded in paraffin were sliced into sections and stained with HE, and sirius red using standard protocol for histopathology analysis of liver. Stained slides were observed under a BZ-9000 BioRevo digital microscope (Keyence Corp., Osaka, Japan), and were analyzed using ImageJ.

3.2.6. Apoptosis TUNEL assay

Apoptotic cells *in situ* were detected in paraffin embedded liver sections using DeadEnd Colorimetric TUNEL system (Promega Corp., Madison, WI, USA) according to the manufacturer's instruction. Sections were counter stained with hematoxylin. Stained slides were observed under a BZ-9000 BioRevo digital microscope (Keyence Corp., Osaka, Japan), and were analyzed using ImageJ.

3.2.7. Total RNA extraction and microarray analysis of liver

Total RNA extraction and microarray analysis were performed as described in the Section 2.2.5.

3.2.8. Gene expression analysis

The total RNA of liver tissues was extracted as described in Section 2.2.5. First-strand cDNA was amplified from the total RNA (100 ng) using SuperScript III Reverse Transcriptase kit (Invitrogen, Carlsbad, CA, USA). The quantification of total RNA and cDNA was measured on NanoDrop 2000 spectrophotometer (Thermo Scientific, Wilmington, DE, USA). Real-time quantitative PCR of target gene expression was assayed by TaqMan predesigned primers (Applied Biosystems, Foster City, CA, USA) and TaqMan Gene Expression Master Mix (Life Technologies, Carlsbad, USA) using the 7500 Fast Real-Time PCR System (Applied Biosystems, Foster City, CA, USA). The following primers were bought from Applied Biosystems: transforming growth factor beta 1 (*Tgfb1*) (Mm01178820_m1), collagen type 1 alpha 1 (*Colla1*) (Mm00801666_g1), and glyceraldehyde-3-phosphate dehydrogenase (*Gapdh*) (Mm99999915_g1). The $2^{-\Delta\Delta Ct}$ method was applied to calculate the relative mRNA expression levels using *Gapdh* as a housekeeping endogenous control.

3.2.9. Western blotting

Western blotting was performed as described in the Section 2.2.7. Primary antibodies: rabbit anti- α SMA (ab5694), and mouse anti-GAPDH (ab8245), and secondary antibodies: Alexa Fluor® 488-conjugated donkey anti-rabbit (ab150073), Alexa Fluor® 594-conjugated donkey anti-mouse (ab150108) were purchased from Abcam.

3.2.10. Statistical analysis

All data are expressed as the mean \pm SEM. Normality test was performed to confirm the normal distribution. A one-way analysis of variance (ANOVA) followed by Tukey's post hoc test was applied to assess the statistical significance of difference among the treatment groups. A value of $p < 0.05$ was considered as significant for all results. Statistical analyses were performed using IBM SPSS Statistics version 24.0.

3.3. Results

3.3.1. Isorhamnetin treatment improved histopathologic condition of fibrosis and apoptosis in liver with NASH

One of the NASH features that distinguish it from benign steatosis is hepatic fibrosis characterized by excessive deposition of ECM. To address this hallmark, we evaluated collagen deposited area stained with sirius red stained (Figure 3.1.a). NASH-induced liver showed greater collagen deposition surrounding portal vein than in those of CTL group. Interestingly, NASH-induced mice when treated with isorhamnetin had diminished collagen. Morphometric analysis further confirmed that isorhamnetin treatment reduced deposition of collagen from 2.25 to 1.17% of total surface ($p < 0.001$ vs. NASH) (Figure 3.1.c), indicating that isorhamnetin treatment efficiently improved fibrotic condition of NASH-induced liver.

Moreover, highest number of apoptotic cells was found in NASH-induced mice compared to other two groups revealed by TUNEL assay (Figure 3.1.b, d). These findings collectively suggest that isorhamnetin treatment alleviated histopathologic condition of NASH-induced liver by reducing steatosis, fibrosis, and number of apoptotic cells.

3.3.2. Changes in oxidation reduction process and activation of HSCs

Oxidative stress is well known to be one of the main drivers in the development of fibrosis and cell death by causing cell damage and liver injury [24]. In response to hepatic insults and increased secretion of pro-inflammatory cytokines such as TGF β ,

HSCs become activated from quiescent state which leads to excessive deposition of extracellular matrix (ECM) and eventually scarring. When all upregulated redox gene expressions (57 genes in total) occurred in NASH were compared with NASH+ISO in heat map, important proportion of genes (41 genes) expression was decreased in NASH+ISO (Figure 3.2.a).

To yield a clearer understanding of the effect of isorhamnetin on redox-mediated processes, we further analyzed genes implicated in HSCs activation, proliferation, Nrf2-mediated oxidative stress and apoptosis. The mean expression level of genes involved in HSC activation such as transforming growth factor beta receptor 1 (*Tgfb1*), and several types of collagen was significantly greater in NASH, and decreased to near CTL level in NASH+ISO, indicating the activation of HSCs was decreased after isorhamnetin treatment (Figure 3.2.b). Among 41 genes averaged in proliferation process such as several genes encoding cell division cycle-associated proteins (*Cdca2*, *Cdca3*, *Cdca8*), globally upregulated genes were overrepresented in NASH, while downregulated in NASH+ISO. Nrf2-mediated oxidative stress markers including 38 genes were slightly ameliorated in NASH+ISO compared to NASH. Similarly, genes included in regulation of apoptosis encoding such as TNF-receptor superfamily proteins (*Tnf*, *Tnfrsf11b*, *Tnfrsf12a*, *Tnfrsf21*), Fas cell surface death receptor (*Fas*), and caspases (*Casp2*, *Casp6*, *Casp7*) were higher in NASH compared to NASH+ISO.

3.3.3. Isorhamnetin prevented liver damage and activation of TGF β -mediated profibrotic gene expression

We found that both ALT and AST levels in serum were increased significantly in NASH-induced mice compared with those of in CTL counterpart ($p < 0.001$ for both enzymes). However, NASH+ISO group had significantly decreased ALT and AST enzyme levels when compared with NASH group ($p < 0.01$ and $p < 0.001$ vs. NASH, respectively), suggesting that NASH-induced liver was less injured when treated with isorhamnetin (Figure 3.3.a). Protein level of α SMA, a marker of HSC activation, was markedly increased in NASH compared to CTL, while decreased in NASH+ISO (Figure 3.3.b). Next, we measured the mRNA expression level of *Tgfb1*, and *Colla1*. The results indicated that the NASH+ISO group showed consistently decreased mRNA levels compared to NASH ($p < 0.001$ for both genes) (Figure 3.3.c, d). Our data suggest that isorhamnetin treatment prevented not only HSC activation, but also mitigated oxidative stress and liver injuries in NASH-induced liver.

3.3.4. Adipocytes enlarged but less infiltrated macrophages in adipose tissue of NASH-induced mice treated with isorhamnetin

Serum lipid profile, including TC, and HDL did not show marked difference among all groups. Serum TG level was greater both in NASH and NASH+ISO mice compared with that of in CTL mice (Figure 3.4.a). Adipose tissue to body weight ratio was significantly increased in NASH-induced mice than that of in CTL mice (2.74% vs.

1.47% for NASH vs. CTL, respectively, $p=0.026$), however, the ratio was decreased slightly, but not statistically significant when treated with isorhamnetin (2.74% vs. 2.38% for NASH vs. NASH+ISO, respectively, $p=0.4$) (Figure 3.4.b). Most importantly, HE staining showed accumulation of macrophage infiltration into adipose tissue in NASH-induced mice, although adipocyte hypertrophy did not display visible difference between NASH and NASH+ISO groups (Figure 3.4.c).

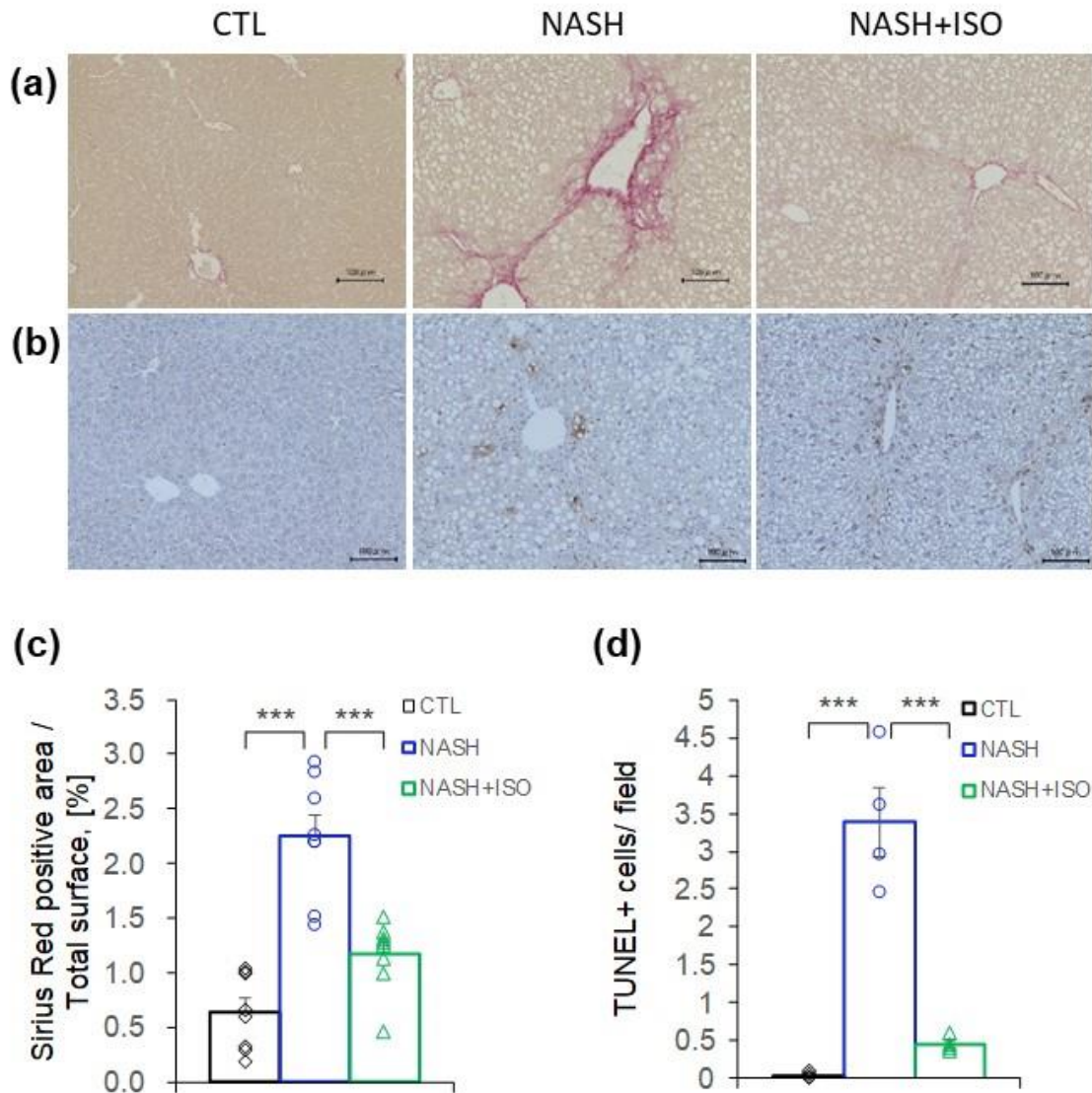


Figure 3.1. Effect of isorhamnetin on fibrosis and apoptosis of NASH-induced mouse liver. Representative microscopic images of Sirius red-stained (a), and apoptotic cells detected by TUNEL staining (b) liver sections (scale bar = 0.1 mm). (c) Quantification of sirius red positive area of liver section (n = 8 / group). (d) Number of TUNEL positive cells per x20 field (n = 4 /group). Data are shown as mean \pm SEM with significance ***p < 0.001.

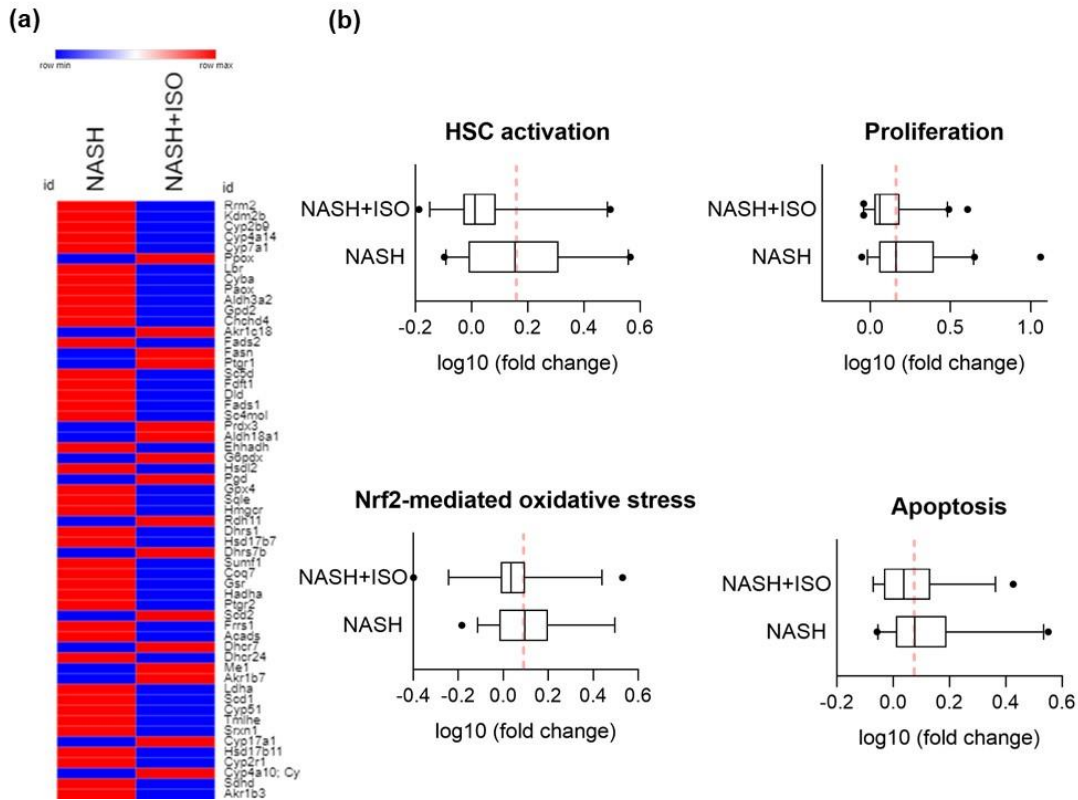


Figure 3.2. Changes in oxidation reduction process and activation of HSCs. (a) Heat map showing DEGs involved in oxidation reduction process between NASH and NASH+ISO compared to CTL group. (b) Box plot with median averaging genes involved in HSC activation (26 genes averaged), proliferation (41 genes averaged), and NRF-mediated oxidative stress (38 genes averaged). Red dash line shows the median of NASH group.

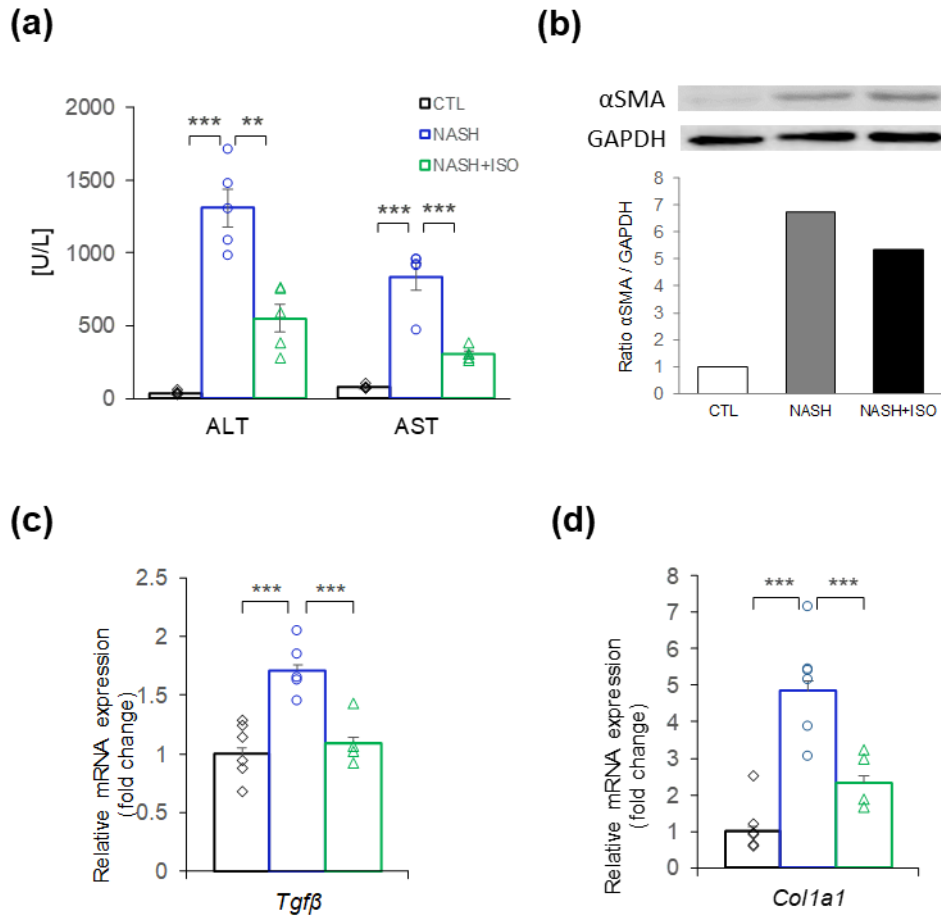


Figure 3.3. Effect of isorhamnetin on liver injury and fibrogenic gene expression. (a) Serum level of ALT and AST measured by automated biochemical analyzer (n = 5 /group, ALT value of NASH vs. NASH+ISO: p = 0.0017). (b) Immunoblot analysis for α SMA in liver tissue and quantification of band intensities normalized to GAPDH. Relative mRNA expression level of *Tgf β* (c) and *Col1a1* (d) genes (n = 4-6 / group) by qPCR analysis. Data are shown as mean \pm SEM with significance **p < 0.01 and ***p < 0.001.

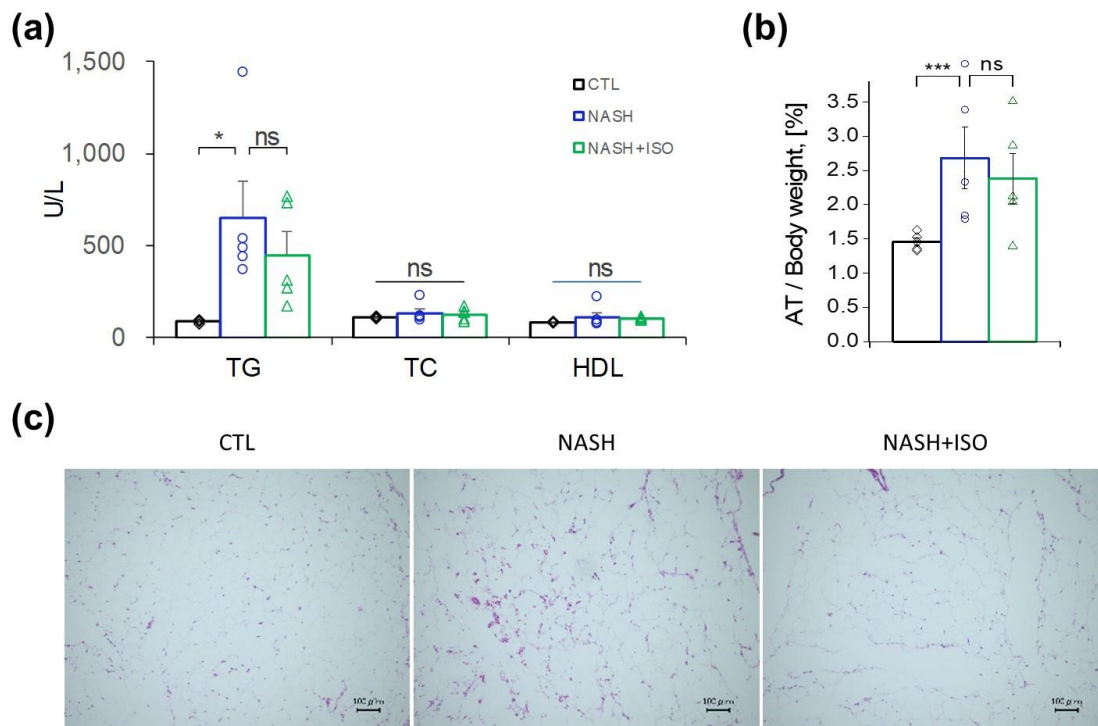


Figure 3.4. Effect of isorhamnetin on adipose tissue and lipid profile in serum. (a) Serum level of TG, TC, and HDL measured by automated biochemical analyzer (n = 5 / group, CTL vs. NASH: p = 0.0215). (b) Adipose tissue on body weight ratio (n = 7 / group). Data are shown as mean ± SEM with significance *p < 0.05, ***p < 0.001 and ns = non-significant. (c) Representative microscopic images of HE-stained adipose tissue sections (scale bar = 0.1 mm).

3.4. Discussion

Liver is susceptible to injuries from multiple insults in the course of development of NASH. It is also well established that consistent damage in liver leads to hepatocyte death by apoptosis and necrosis when liver fails to respond adequately to this pathologic condition [25]. Liver biopsy analysis reveals that in NASH patients the increased number of cells are undergoing apoptosis by both intrinsic and extrinsic pathways [26]. Increased number of apoptotic cells contributes to exacerbate the progression of fibrosis [27]. Thus, at first, we measured serum levels of ALT and AST enzymes as markers of liver injury. These enzyme levels are immediately increased when hepatocytes are subjected to acute injury allowing us to evaluate liver injury state. Isorhamnetin-treated group showed the lower level of ALT and AST compared to NASH, indicating its protective effect against injuries.

We found that treatment with isorhamnetin markedly prevented cells dying through programmed cell death (apoptosis) in liver of NASH-induced mice, suggesting that isorhamnetin might have reversed activation of hepatocyte cell death by preventing liver injury during NASH progression. The isorhamnetin decreased the mRNA level of *Tgfb1* and *Colla1* which is consistent with the reduced collagen deposition in NASH-induced mice, indicating its potential effect to protect liver from fibrosis development and chronic injuries in the course of NASH progression.

Obesity, insulin resistance, type 2 diabetes are all considered as risk factors for development of NAFLD and NASH, which are primarily characterized by an ectopic

accumulation of lipid in liver. Adipose tissue, especially visceral one, is known to be responsible for an elevated lipolysis and systemic inflammation due to insulin resistance resulting in hepatic lipid accumulation and inflammation [28]. As shown histologic analysis, even though adipocyte was enlarged in both NASH and NASH+ISO groups, NASH group has more inflamed adipose tissue revealed by the increased number of macrophage infiltration and NASH+ISO was protected from the inflammation. Thus, reduced accumulation of lipid observed in the livers of isorhamnetin-treated NASH mice might be partly related to its direct effect on white adipose tissue by the alleviation of inflammatory state.

These findings collectively suggest the alleviative effect of isorhamnetin against NASH-related pathologic features including steatosis, injury, and fibrosis. As isorhamnetin is a direct metabolite of quercetin differing by a single methyl group, but able to exert more efficiently anti-NASH effect than quercetin. These findings curiously led us to consider whether the position of methyl group plays an important role in the regulation of its biological activity, and this difference of methyl group possesses more efficient activities. Thus, the structure-activity relationship analysis of five structurally-possible monomethylated derivatives was analyzed for their antifibrotic activities in the next chapter.

Chapter 4

Effect of Isorhamnetin and Its Derivatives on Fibrosis in TGF β -Induced Hepatic Stellate Cells

4.1. Introduction

Flavonoids are natural polyphenols commonly presented in fruits, vegetables, and seeds. They have been known for their beneficial effects against cancers, cardiovascular, and neuronal diseases [29]. But, despite several promising roles of flavonoids, the application of these agents to human has met with only limited success, mostly due to their instability and low rate of oral bioavailability [30]. Several researches have shown that the bioactive forms of flavonoids are the conjugates and metabolites that derived from their parent aglycone forms on absorption. All flavonoids are converted in extensive phase I deglycosylation in the small intestine and further phase II metabolism in the liver providing aglycones to glucuronides, O-methylated forms, and sulphates. These circulating metabolites of flavonoids in the body are considered to most probably exert bioactivity and beneficial effects in human organism and animal models.

In addition, depending on the positions reacted substrates, and donor groups, glycosylation, and methylation have different effects. However, the glycosylated flavonoids showed only enhanced solubility and were largely lack of prominent biological activity [31]. Moreover, addition of methyl group in flavonoids could greatly increase their metabolic stability within the organism and facilitate membrane transport resulting in improved absorption and increased bioavailability of flavonoid. Thus, methylated flavonoids have beneficial effect as pharmaceutical agents [32].

Quercetin is one of the most widely studied flavonoids exerting antiproliferation, anti-inflammatory, antioxidant, antifibrogenic, and as well as

cardioprotective effects. Hence, quercetin is rarely found in aglycone form in the plasma after ingestion and circulates usually in conjugated forms [33]. Generally, 20 – 40% of quercetin is methylated in the 3'-position, forming its immediate metabolite - isorhamnetin. Isorhamnetin is also found in nature, in plants and plant-derived foods, and known for its inhibitory effect on proliferation of breast cancer cells, prevent HepG2 cells from oxidative stress insults, as well as attenuation of inflammatory bowel disease (IBD), and inhibits adipogenesis in 3T3-L1 cells [1,2,5]. More recent studies have demonstrated antioxidant, anti-obesity, and antifibrotic effects in rodent models [6,7,23].

In addition, quercetin has more than one hydroxyl groups in its aglycone chemical structure. Addition of methyl group in different positions of its structure leads to five mono-methylated derivatives of quercetin, such as isorhamnetin, 3-*O*-methyl quercetin, azaleatin, tamarixetin, and rhamnetin. Even though large number of studies on biological effects of quercetin has been conducted, there is still limited biological evidences on the effects of the methylated derivatives of the flavonoid quercetin.

Of note, to mention that different cell types show different results in response to flavonoids treatment. Therefore, the absorption of flavonoids and conjugation of metabolites, determines their biological activities, meaning not only the form of flavonoids but also the cell types which is been absorbed [31]. In the previous chapter, we have reported the antifibrogenic effect of isorhamnetin in the liver of a steatohepatitis mice model. Liver fibrosis is a hepatic chronic disease characterized by the excessive accumulation of extracellular matrix (ECM) which can progress to

irreversible scarring and end-stage liver diseases if the injury is persistent and chronic. However, hepatic fibrosis is orchestrated basically by the hepatic stellate cells (HSC), a resident cell population comprising one-third of the nonparenchymal cells and five percent of the total liver cells in human liver in physiologic condition. Chronic hepatic injury can be caused by different types of viral infections, metabolic disorders, heavy alcohol consumption, and NASH leads to transdifferentiation of HSCs from their quiescent state into more proliferative, migratory, and more contractile myofibroblasts to increase the production of ECM consisting mainly of collagen which leads to fibrosis development, irreversible scarring, and subsequent liver damage [34–36]. Even though various drugs have been demonstrated possessing antifibrotic activity *in vitro* and in animal models, any of these candidates have been shown to be effectively applicable in human subjects. Thus, recent interests are evolving in strategies to therapeutically accelerate the deactivation of HSCs activity in the treatment of liver fibrosis.

In this study, based on *in vivo* results from the previous chapters we investigated the effect of five different methylquercetin derivatives and quercetin on the activation and proliferation of HSCs and on the production of ECM using TGF β -induced HSC-T6 cells to elucidate their structure-activity relationship as antifibrosis compounds.

4.2. Materials and Methods

Detailed methodology of assays was explained in the endnote, and mentioned elsewhere [37].

4.2.1. NMR data of methylated quercetin

Five different mono-methylated quercetin derivatives: ISO, AZA, 3MQ, TAM, and RHA were synthesized from commercially available quercetin in reference to reports [38]. All synthesized mono-methylated quercetin was in good agreement with reported data [39–42]. Chemical structure and purity of each compound were shown in Figure 4.1. NMR data were in the endnoteⁱⁱ.

4.2.2. Chemicals and reagents

A stock solution of 100 mM for each compound was prepared by dissolving in DMSO and stored at -20°C until use. Working solution (treatment) was prepared before use by diluting the stock solution in the culture media. Thus, the final concentration of DMSO in the medium did not exceed 0.04% for 40 μM, and 0.02% for 20 μM of treatment. Human recombinant TGFβ1 was purchased from Peprotech (NJ 08553, USA), reconstituted according to the manufacturer's instruction, and stored at -20°C until use. Anti-α smooth muscle actin (ab5694), anti-collagen I (ab34710), AlexaFluor 488 labeled donkey anti-rabbit (ab150073) antibodies were purchased from Abcam (Tokyo, Japan). ProLong Diamond antifade mountant with 4',6-Diamidino-2-Phenylindole (DAPI: double stranded DNA staining) was purchased from Invitrogen (ThermoFisher, USA).

4.2.3. Cell line and culture condition

From Millipore (Millipore, CA, USA) HSC-T6 cells were obtained, and

maintained according to the manufacturer's instruction, cells were cultured and passaged in DMEM-High glucose (D5796, Sigma-Aldrich, USA) containing 2.5 mM L-Glutamine supplemented with 10% FBS (Gibco, USA) and penicillin and streptomycin (5000 µg/ml, 5000 IU/ml respectively) at optimum condition, and were sub-cultured after reaching at 90% confluence. We used cells of passages in 3 - 8 for cell assays.

4.2.4. Cell proliferation assay

HSCs were prepared in seeding at a density of 1×10^5 cells/ml in a 96-well plate. For 3-(4,5-dimethylthiazol-2-yl)-2,5-diphenyltetrazolium bromide (MTT) assay we treated cells with different concentrated derivatives for 12 hours and 24 hours of incubation. Sodium dodecyl sulfate (SDS) solution was used to dissolve formazan crystals, and absorbance was measured at 570 nm, and proliferation was calculated. Details are explained in the endnoteⁱⁱⁱ.

4.2.5. Immunofluorescence-staining analysis

HSC-T6 cells were cultivated at a density of 5×10^4 cells/ml in 6-well plate and treated with TGFβ with or without compound treatment to induce fibrosis. Following immunofluorescence staining standard protocol, αSMA and Col1 were detected. Details are explained in the endnote^{iv}.

4.2.6. Real-time reverse transcription polymerase chain reaction (RT-PCR) analysis

HSC-T6 cells were seeded with a density at 1×10^5 cells/ml in 6-well plate and incubated for 12 hours. Cells were subsequently treated with 2 ng/ml of TGF β and with the compound for 1 h. Total RNA was extracted as described in the Section 2.2.5. Reference of primers and protocols are detailed in the endnoteⁱ.

4.2.7. Statistics

Significance of difference between the treated groups was determined using Student's *t*-test (two-tailed). All data were expressed as the mean \pm standard deviation (SD) or standard error of the mean (SEM), significance was considered at $p < 0.05$. For multiple comparisons ANOVA followed by Dunnett's post-hoc test among controls (NC and PC) and derivative-treated groups was conducted. For statistical analysis we used IBM SPSS software (ver. 24.0). All graphics were prepared in Microsoft Excel 365.

4.3. Results

4.3.1. Optimizing TGF β induction in HSC-T6 for fibrosis *in vitro* model

HSC activation drives a main pathway implicated in liver fibrogenesis. Insults such as drugs, viral infection, and liver chronic diseases including NASH cause HSCs to be activated resulting in the increase of proinflammatory cytokines level. These cytokines further trigger intracellular signaling pathways which will accelerate the HSC activation process. TGF β and TGF β /Smad pathway are well established to be implicated in liver

fibrogenesis as a potent profibrotic factor and its downstream mediators [43]. Once activated HSCs are modulated phenotypically by becoming mobile, fibroblast-like and more proliferative, and start secreting α SMA that induces ECM molecules deposition. For its known role, TGF β was used to induce HSC-T6 activation in our fibrosis model. To determine the suitable TGF β concentration for the induction of *in vitro* fibrosis, we treated HSC-T6 with different TGF β concentration in our preliminary study. After 24 hours of incubation, α SMA and Col1 were stained by immunofluorescence detection (Figure 4.2). Accumulation of α SMA moderately increased at the dose 0.5 ng/ml of TGF β and greatly increased from 2 ng/ml, although any difference was not found in TGF β concentration of 2 - 4 ng/ml (Figure 4.2). TGF β treatment at the concentration of 0.5 ng/ml for 24 hours resulted increase in deposition of Col1 compared with untreated cells. This increase was dose dependent up to 4 ng/ml (Figure 4.2).

Expression of *Acta2* and *Colla1* mRNA levels were determined after treated with TGF β for 24 hours (Figure 4.3.a, b). Important dose-dependent increase in *Acta2* mRNA level was observed from 2 ng/ml of TGF β . *Colla1* mRNA augmented slightly along with the increase of dose, however, it did not reach a statistical significance.

We also investigated proliferative effect of TGF β treatment on the rat stellate cells. Although HSC-T6 proliferation rate was not noticeably altered compared to untreated cells after 12 hours of TGF β treatment at the dose between 0.5 ng/ml and 8 ng/ml (Figure 4.4). Therefore, we considered 2 ng/ml TGF β is the most suitable concentration that can stimulate fibrosis without altering proliferation rate of stellate

cells.

4.3.2. Antiproliferative effects on HSC-T6 after TGF β induction

Activated HSC-T6 acquire more proliferative and mobile properties which leads eventually an aberrant production of ECM. Therefore, to investigate the effect of derivatives on HSC-T6 proliferation rate, cells were treated with compounds with different concentrations for different period of time. Subsequently, HSC-T6 viability was determined (Figure 4.5). Although except ISO after 6 hours of treatment, anti-proliferation effect of compounds tended to be weakened in a dose-dependently (Figure 4.5.a). When treated for 12 hours, comparable to untreated cells (NC) the proliferation rate was dropped drastically in ISO-treated cells. ISO at 40 μ M more effectively inhibited proliferation rate (Figure 4.5.b), and the dose of 80 μ M after 24 hours markedly inhibited the HSC-T6 proliferation rate (Figure 4.5.c). QCT, ISO, and 3MQ showed efficient inhibitory effect starting at 10 μ M time- and dose-dependently. Inhibitory effect of other derivatives namely RHA, TAM, and AZA start been observed at 80 μ M over 12 hours of incubation. Based on these findings, 20 μ M and 40 μ M of compound doses were used for the next experiments.

4.3.3. Effect of methylated derivatives on Col1 and α SMA production

Next, to discover each compounds effect on the production of Col1 and α SMA after TGF β -induction, TGF β -induced HSC-T6 cells were treated at 20 μ M and 40 μ M of

compound for 24 hours. Immunofluorescence staining for Col1 and α SMA was performed (Figure 4.6). We found that greatly decreased production of α SMA in all compound-treated HSC-T6 compared to a positive control (PC). But among all compounds, ISO, QCT, RHA, and 3MQ efficiently decreased α SMA production at the dose of 20 μ M, and more effectively at 40 μ M showing a dose-dependent efficiency. Inhibition by TAM and AZA were slightly lower than other derivatives. However, α SMA was greatly reduced compared to positive control. Col1 was also evaluated after treated for 24 hours to analyze compounds inhibitory effect on the development of ECM. Interestingly, TAM, AZA, and 3MQ treatments showed decreased Col1, however, it was slightly inhibited in ISO-treated HSCs. Compared to untreated control RHA and QCT showed a slight decrease in collagen deposition (Figure 4.6).

4.3.4. Effect of methylated derivatives on pro-fibrotic gene expression

Previous results showed that derivatives efficiently inhibited the accumulation of α SMA after 24 hours of incubation with derivatives in TGF β -induced HSCs. Next, we sought to confirm whether their inhibitory effect can be exerted on *Acta2*, tissue inhibitor of metalloproteinase-1 (*Timp1*), and *Colla1* gene expression level. As shown in Figure 4.7.a, TGF β significantly increased the mRNA level of *Acta2* after 1 hour of incubation. When treated simultaneously with compounds, RHA, ISO, and QCT showed efficient downregulation of the *Acta2* gene mRNA level. Surprisingly, AZA, 3MQ, and TAM failed to exert inhibition effect. Treatments with 3MQ and ISO for 6 hours decreased the

Acta2 mRNA expression level. Moreover, AZA showed a tendency to decrease *Acta2* gene expression after 6 hours, although its level was still higher than NC. In contrary, QCT and TAM increased *Acta2* expression significantly after 6 hours when compared to NC. *Colla1* mRNA was transiently increased up to 1h and but decreased after 6 hours when treated with RHA, QCT, 3MQ, and AZA (Figure 4.7.b). After treated with 3MQ for 6 hours, *Colla1* was significantly dropped to the level of the control. On the other hand, *Colla1* remained higher in the cells treated with TAM and ISO. Furthermore, *Timpl* was increased significantly in TGF β -induced cells after 6 hours (Figure 4.7.c). *Timpl* mRNA level was inhibited by ISO, RHA, QCT, and TAM treatments. However, AZA and 3MQ derivatives did not show inhibitory effect on *Timpl* mRNA gene expression level.

4.4. Discussion

In this chapter, we demonstrated that mono-methyl quercetin derivatives differing by their methyl group position had different biological effects on profibrotic gene expression and proliferation in TGF β -induced rat stellate cells. Our preliminary results suggested that determining suitable dose and time to use in TGF β -induced stimulation of fibrosis *in vitro* model is a decisive parameter to carry out the experiments on the effect of compounds adequately.

Although related pathways and underlying cellular signaling in the setting of liver fibrosis have been extensively studied, TGF β -induced axis remains as the main target for therapeutic strategy [44,45]. Highly increased TGF β in liver injury state activates HSCs, in turn, HSCs are the main source in the development of fibrosis. HSCs undergo phenotypic modification from quiescent and non-proliferative resting state to activated state accompanied with increased proliferation rate, and excessive ECM production. The most emerging therapeutic strategies are intended to retardate HSCs activation and prevent them to become proliferative, and promote degradation of ECM to resolve liver fibrosis [46,47]. But the fact that targeting directly TGF β is not considered as a promising approach because of its off-target unpredictable cell response as well as its involvement in physiologic and pathologic regulation of liver [48]. Therefore, a compound that regulates specifically TGF β -induced pro-fibrotic pathways attracts attention for eventual clinical application.

Cumulated findings showed that plant extracts and various flavonoids possess biological activity against hepatic fibrosis [23,49,50]. Yang and colleagues reported that CCl₄-induced liver fibrosis were inhibited by isorhamnetin treatment, and the downstream molecules of TGFβ pathway such as phosphorylation of Smad 2/3 in rodent primary HSCs and human LX-2 were downregulated [23]. Li et al. demonstrated that ISO significantly inhibited lung cancer cells proliferation by regulating apoptosis [51]. Our findings showed that 3MQ and isorhamnetin had strong inhibitory effects on HSC-T6 proliferation. These findings were also supported by the reduced expressions of *Timp1* and *Acta2*. Moreover, methylated position of 3MQ and isorhamnetin are conformationally located closer compared to the remaining derivatives that suggests the functional role of methylation on C-3' and C-3 positions against fibrogenesis.

Kawada et al. reported that quercetin also prevents the HSCs activation by downregulating *Acta2* expression and subsequently, inhibits the serum-dependent proliferation by dose-dependent manner [49]. Wu and colleagues demonstrated that hepatic fibrosis caused by either by injecting liver toxin (CCl₄) or ligating the bile duct could be ameliorated by quercetin treatment in mice via reduction of autophagy and downregulation of stellate cell activation [8]. According to our findings, quercetin could reduce *Timp1* and *Colla1* mRNA gene expression slightly, but did not affect *Acta2*, after incubated with TGFβ for 6 hours. Collectively, our results support along with previous reports on the inhibition effects of quercetin on proliferation of HSCs. Treatment with TAM and AZA did not efficiently inhibit *Colla1* and *Acta2* mRNA expression level

when compared with positive control. This finding shows that the hydroxyl group in C-5 and C-4' positions are needed to their efficient activities, because the addition of methyl group on these positions weakened their activities.

Of note, technically, we expected that the immunostaining of α SMA reveals a dense network of fibers in HSCs after the induction by TGF β as a marker of the HSCs activation. However, we could visualize the small sized and dotted nuclear accumulation of α SMA stained by the antibody even though *Acta2* gene expression increased significantly by qPCR analysis. To confirm the relevance of stained α SMA following the HSC activation, alternative proteins related to the ECM and fibroblasts such as vimentin, or different induction method could be considered.

Although the molecular function of all derivatives remained to be clarified, collectively, our findings demonstrated that the biological activity of monomethyl derivatives on fibrosis development is different than quercetin. Moreover, its antifibrotic effects can be enhanced by modulation of -CH₃ group on functionally important positions.

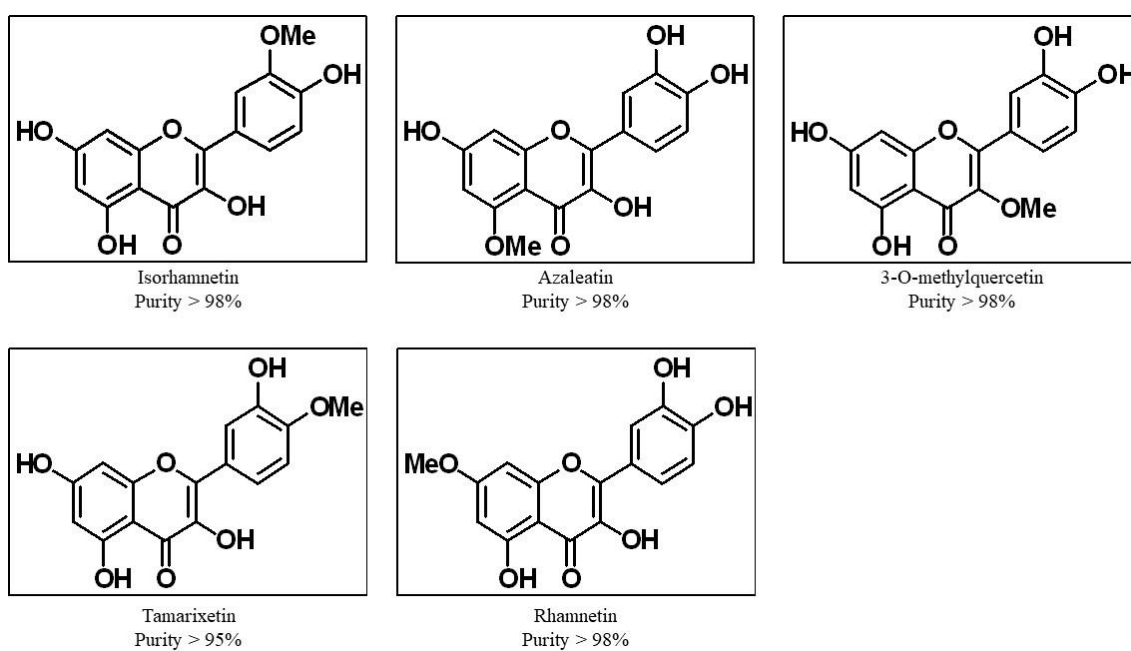


Figure 4.1. Chemical structure and purity of synthesized compounds.

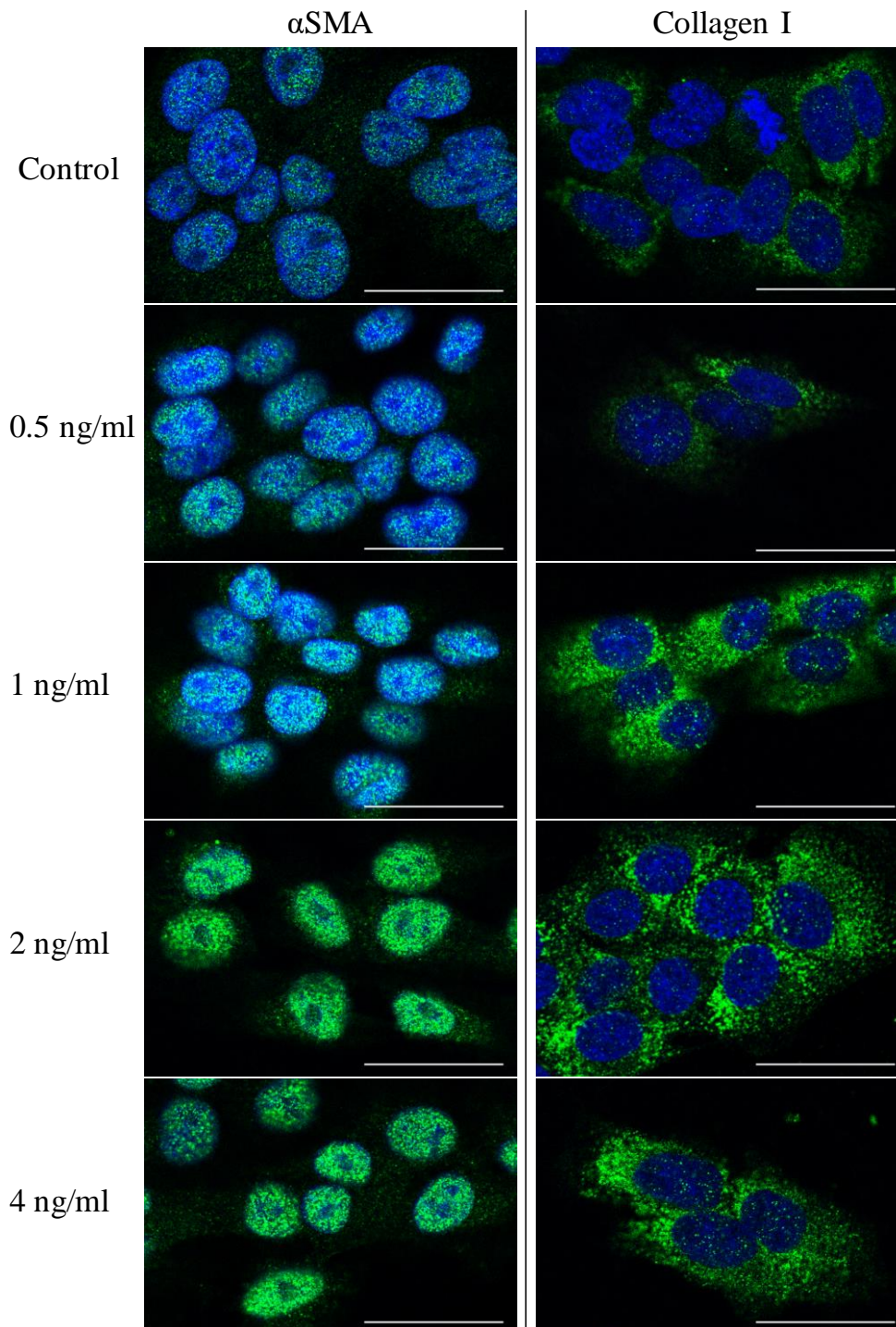


Figure 4.2. Immunodetection of Collagen I and α SMA in TGF β -induced HSCs. Cells were incubated with different concentration of TGF β for 24h, and α SMA (green, 1st column), collagen I (green, 2nd column) and nucleus (blue) were detected by immunofluorescence staining (Scale bar = 30 μ m). Control represents non-treated negative control.

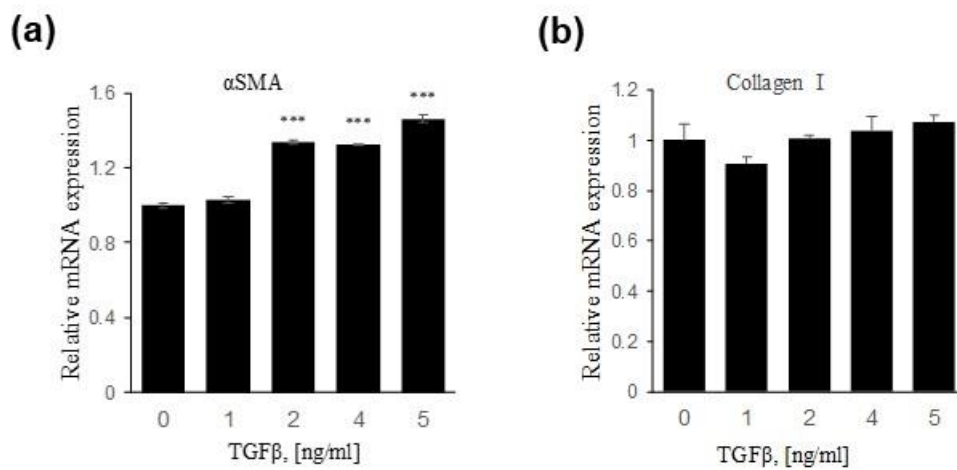


Figure 4.3. Gene expression of α SMA and Collagen I in TGF β -induced HSCs. Cells were incubated with different concentration of TGF β for 24 h. Relative mRNA expression level of α SMA (a) and collagen type I (b) genes by qPCR analysis. Data are shown as mean \pm SEM of at least three independent experiments with significance *** $p < 0.001$ vs. non-treated control.

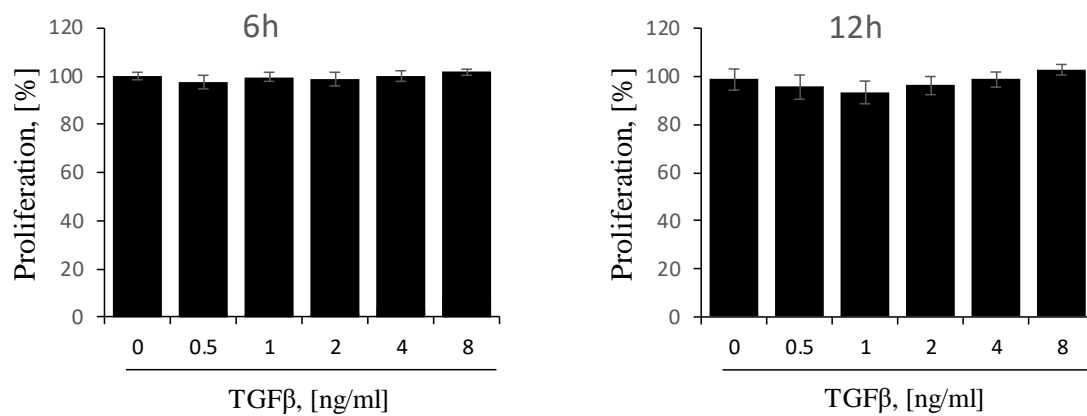


Figure 4.4. Effect of TGFβ on proliferation of HSCs. Cells were incubated with different concentration of TGFβ for 6 and 12 h, and cell proliferation rate was determined by MTT assay. Cell proliferation rate of non-treated cells was set as 100% according to the calculation explained in the section 4.2.4. Data are shown as mean ± SD of at least three independent experiments.

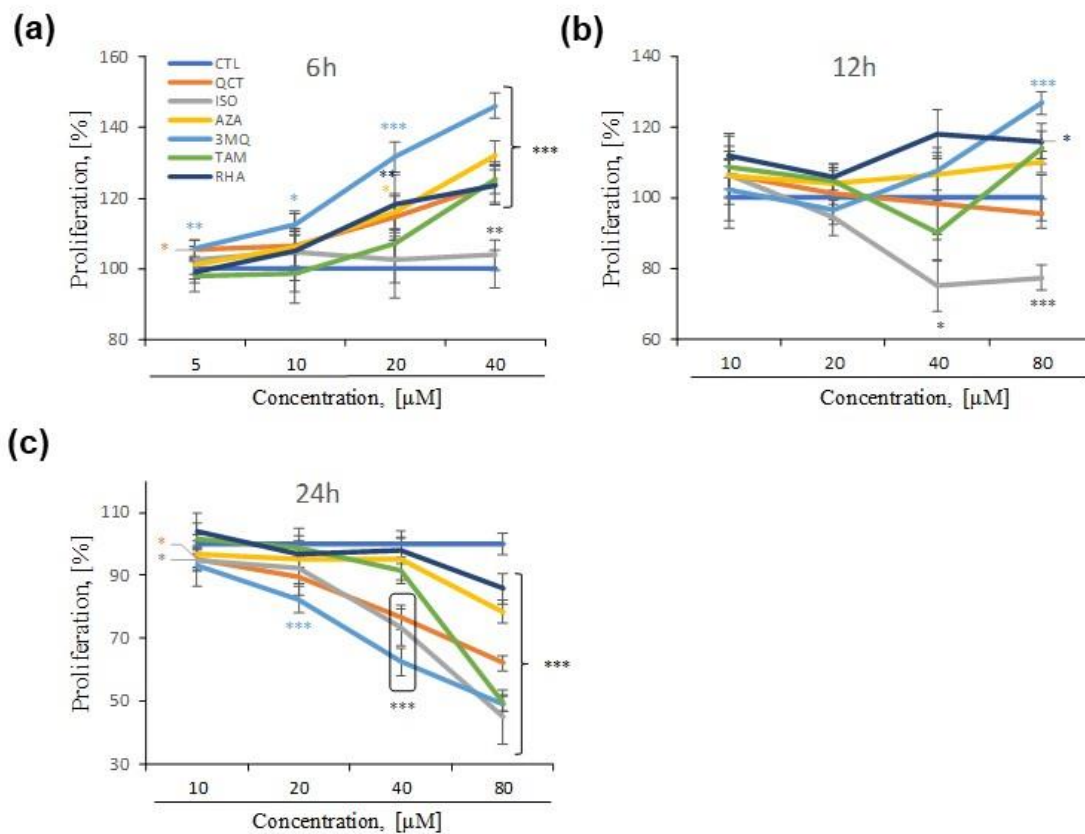


Figure 4.5. Inhibitory effect of compounds on proliferation of HSCs. Cells were incubated with different concentration of compound for 6 h (a), 12 h (b), 24 h (c), and cell viability was measured by MTT assay. Cell proliferation rate of non-treated cells (CTL) was set as 100% in each condition according to the calculation explained in the section 4.2.4. Data are shown as mean \pm SD of at least three independent experiments with significance * $p < 0.05$, ** $p < 0.01$ and *** $p < 0.001$ vs. non-treated control (CTL).

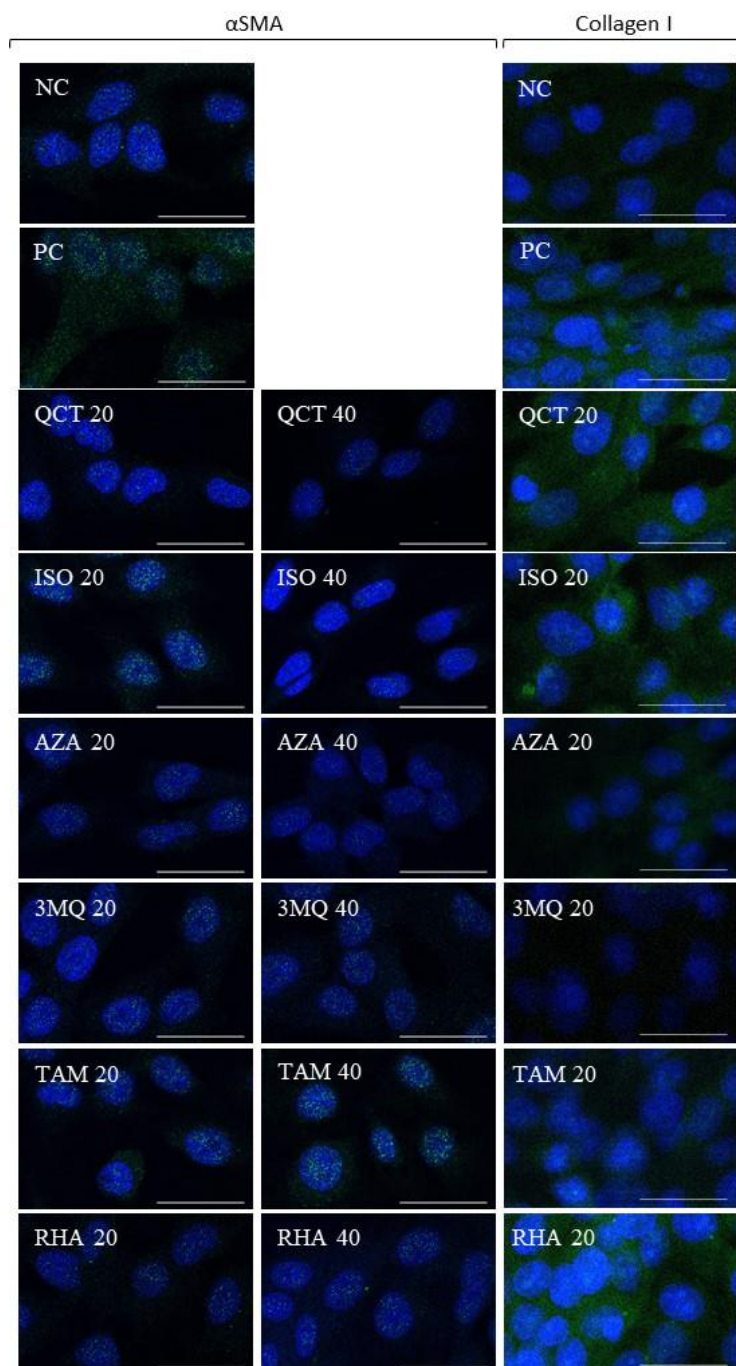


Figure 4.6. Inhibitory effect of compounds on production of α SMA and Collagen I in TGF β -induced HSCs. Cells were incubated with 20 μ M and 40 μ M concentration of compound in the presence of 2 ng/ml of TGF β for 24 h, and α SMA or Collagen I (green) and nucleus (blue) were detected by immunofluorescence staining (Scale bar = 30 μ m). NC – non treated negative control, PC – treated with 2 ng/ml of TGF β positive control.

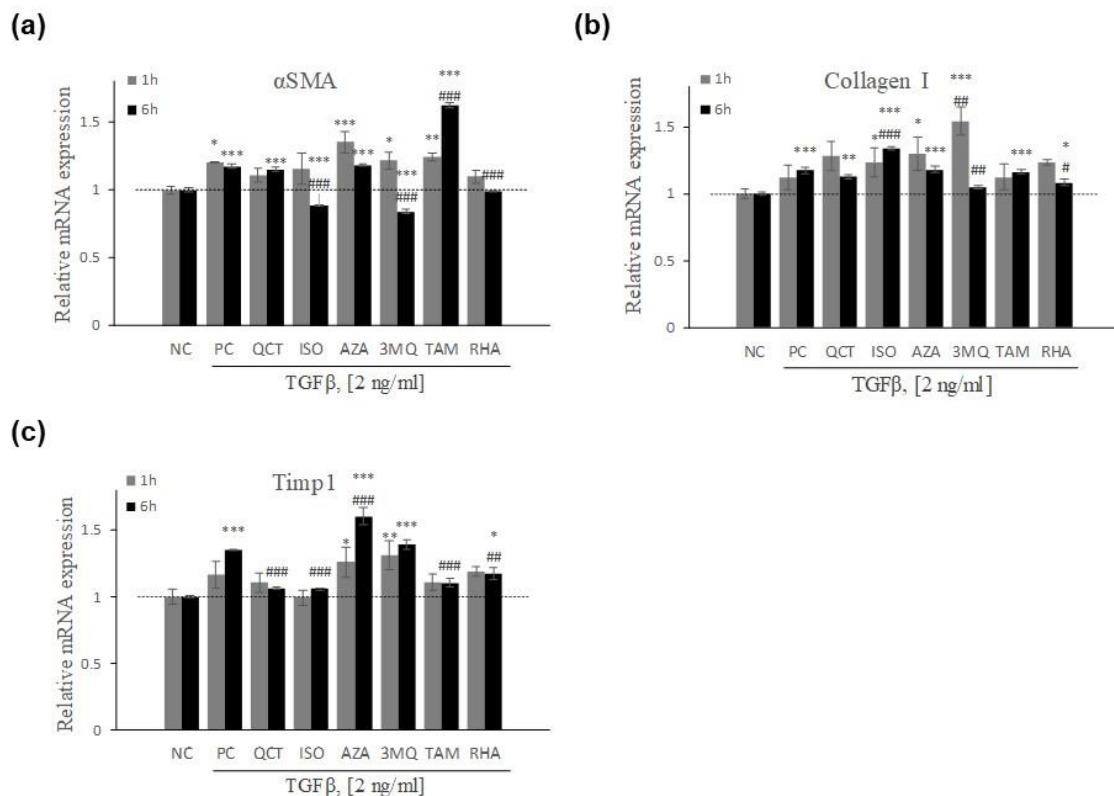


Figure 4.7. Inhibitory effect of compounds on pro-fibrotic gene expression in TGFβ-induced HSCs. Cells were treated with 2 ng/ml of TGFβ and 20 μM of compound for 1 and 6 h. Relative mRNA expression level (fold change) of (a) *Acta2*, (b) *Colla1*, and (c) *Timp1* were determined by real time qPCR. Data are shown as mean ± SEM of at least three repetitions with significance *p < 0.05, **p < 0.01 and ***p < 0.001 vs. non-treated, non-induced control (NC); and # p < 0.05, ##p < 0.01 and ###p < 0.001 vs. TGFβ-induced positive control (PC) by ANOVA followed by Dunnett's post-hoc test. Horizontal dash line shows the level of NC. Gene expression was normalized to *Gapdh* as mentioned in the section 4.2.6.

Chapter 5

General Discussion

Researchers still have been seeking an effective drug although the underlying molecular mechanism responsible for etiology of NASH is not completely elucidated yet. Several studies showed curative and preventive effects of natural flavonoids against the liver diseases [8,52]. Recently developed rodent NASH model, that we used in our study, was able to show main hallmarks of human-like NASH, including liver steatosis, injury and apoptosis, and fibrosis. This advantage allowed us to study the effect of isorhamnetin not only in liver itself, but also in systemic level. In this study, we demonstrated that oral administration of isorhamnetin could consistently alleviate pathologic features of NASH when compared to non-treated NASH-induced mice, even though the treatment did not lead to its complete cure.

Liver steatosis, inflammation, and fibrosis are interrelated, and are likely to aggravate each other by positive feedback leading to progression of NASH [28]. Lipid accumulation in liver precedes in the setting of NASH and may come from three main sources: around 60% from fat-rich diet, 10-20% from lipolysis of adipose tissue, and 20-30% from hepatic DNL [14,53]. In current clinical practice, diet source and lipolysis of adipose tissue can be controlled up to certain extent by managing diet regime combined with pharmacological strategies. In NAFLD patients, DNL pathway in liver is constantly activated because of insulin resistance and contributes to exacerbation of hepatic steatosis [15–17]. Main regulator of DNL pathway is insulin-induced SREBP1c which triggers its downstream gene expressions required for fatty acid synthesis. We found that isorhamnetin treatment of NASH-induced mice could attenuate DNL pathway by

regulating lipogenic key transcription factor, SREBP1c, which, in turn, downregulated lipogenic enzymes. This result correlates with the histological findings of reduced hepatic TG content and intrahepatic lipid accumulation in isorhamnetin-treated NASH mice compared to untreated NASH mice. It is seemingly possible that the inhibition of DNL pathway may be resulted in the alleviation of liver steatosis by 20-30% as the mRNA expression level of *Apob* was not differed by the isorhamnetin treatment, excluding the increased activity in TG transportation out of liver. SREBP1c is activated following the cleavage in Golgi and matured in endoplasmic reticulum. Over activation of SREBP1c induces endoplasmic reticulum stress which associates with liver steatosis due to increased oxidative stress [54]. Hepatic lipid content was reduced by isorhamnetin treatment from 37% to 23% which brings NASH-induced liver back to mild steatosis category (5-33% as mild, and 34-66% as moderate) according to steatosis grade of NAS score [55]. On the other hand, at systemic level isorhamnetin was also reported to improve glucose metabolism and insulin sensitivity, and protect against lipid peroxidation in diet-induced obese mice and streptozotocin-induced diabetic rats [56].

Reduced mRNA expression of *Tgfb1* and *Coll1a1* by isorhamnetin suggests that isorhamnetin may exert its biological activity on HSCs and macrophages, which are the main sources of TGF β secretion and TGF β -mediated production of collagen in ECM. Yang et al. reported that isorhamnetin isolated from *Oenanthe javanica* exerted anti-fibrotic effect in mice liver with CCl₄-induced fibrosis by preventing the activation of TGF β -induced smad2/3 pathway [23]. In our study, we did not exclude possible

inflammatory insults from adipose tissue and hepatic steatosis-related intrahepatic deregulation of gene expression since the ‘second hits’ possibly act as positive feedback to exaggerate ‘first hits’. In this study, we showed that isorhamnetin could prevent the activation of TGF β -mediated fibrogenesis in NASH-induced mice. Additionally, release of apoptotic bodies derived from injury-induced parenchymal cell apoptosis, activation of immune cells due to systemic inflammation, signaling from Kupffer cells, and lipid peroxidation are considered as fibrogenic factors leading HSCs to activation [57]. Chronic fibrotic state and hepatic cell death by apoptosis are positively correlated with the severity of NASH [26,27]. By mitigating fibrosis and liver injury, longer period of isorhamnetin treatment may bring NASH-induced liver back into more fatty liver-like condition.

Lipid profile measured in non-fasting serum demonstrated insignificant difference between treated and non-treated NASH-induced mice due, at least in part, to consumption of HFD. Similar studies that used flavonoids to treat HFD-induced metabolic disorders in rodents also noted indifference of lipid profile in serum [9]. However, adipose tissue of NASH-induced mice was more inflamed, as evident by the increased number of macrophage infiltration, than those of isorhamnetin-treated mice. On that basis, insignificant change in adipose tissue mass of isorhamnetin-treated mice could be explained by improved glucose uptake and increased insulin sensitivity. Further research is required to explain the long-term effect of isorhamnetin on adipose tissue. Recent studies that used 4-week of treatment with isorhamnetin or isorhamnetin rich plant

extract, showed reduced adipose tissue and body weight accompanied with ameliorated systemic inflammation in diet-induced mice or *db/db* mice [6,58].

Besides their common protective effects on liver steatosis and fibrosis, interestingly, an addition of single methyl group which distinguishes isorhamnetin from quercetin makes isorhamnetin more adequate in absorption and slower in elimination from serum [10]. Thus, our aim was to determine whether there is any structure-activity relationship of the mono-methylation and its effect on fibrogenesis by comparing all possible monomethylated quercetin derivatives including isorhamnetin and quercetin in *in vitro* system. Our findings in Chapter 4 suggested that isorhamnetin, 3-O-methylquercetin, and rhamnetin were stronger in inhibition of fibrogenesis. Structurally, the hydroxyl group in C-5 position, which is common in these three derivatives, seemed essential in exerting their activity because the methylation on this position, the case of azaleatin, led to its loss of antifibrotic activity. In addition, the treatment with tamarixetin – methylated on C-4' position, failed to inhibit fibrogenic markers effectively. The fact that the derivatives methylated on C-3', C-3, and C-7 position or ISO, 3MQ, and RHA respectively, showed the similar effect reveals that not only isorhamnetin but also other methylated derivatives are able to inhibit the development of fibrosis. Manifestly, further investigation is needed to clarify which position is crucial to methylation in mediating its activity more effectively, and what role it plays in the stabilization, metabolization, and absorption of the derivative. Moreover, the antifibrotic effect of not only mono-methylation, but also di-, tri-, quad-, and penta-methylations cannot be excluded from the

hypothesis and remains as an interesting research direction to investigate.

Altogether, our results demonstrated that isorhamnetin elicits beneficial effect on hallmarks of NASH by improving steatosis, injury, and fibrosis in a novel human like NASH-induced mice. This hepatoprotective effect of isorhamnetin was correlated to the inhibition of DNL and fibrogenic gene expressions; alleviation of liver TG content; and diminution of hepatic collagen deposition accompanied with the reduced number of apoptotic hepatocytes. Thus, isorhamnetin can be a novel candidate for the consideration of additional compound in NASH drug development. Further evidence with human NASH will be required to understand the effect of isorhamnetin on NASH.

Endnotes

- i. First-strand cDNA was amplified from the total RNA (100 ng) using SuperScript III Reverse Transcriptase kit (Invitrogen, Carlsbad, CA, USA). The quantification of total RNA and cDNA was measured on NanoDrop 2000 spectrophotometer (Thermo Scientific, Wilmington, DE, USA). Real-time quantitative PCR of target gene expression was assayed by TaqMan predesigned primers (Applied Biosystems, Foster City, CA, USA) and TaqMan Gene Expression Master Mix (Life Technologies, Carlsbad, USA) using the 7500 Fast Real-Time PCR System (Applied Biosystems, Foster City, CA, USA). The following primers were bought from Applied Biosystems: sterol regulatory element binding protein 1 (*Srebf1*) (Mm00550338_m1), fatty acid synthase (*Fasn*) (Mm00662319_m1), acetyl-Coenzyme A carboxylase alpha (*Acaca*) (Mm01304257_m1), apolipoprotein B (*ApoB*) (Mm01545150_m1), and glyceraldehyde-3-phosphate dehydrogenase (*Gapdh*) (Mm99999915_g1). The $2^{-\Delta\Delta C_t}$ method was applied to calculate the relative mRNA expression levels using *Gapdh* as a housekeeping endogenous control.
- ii. Isorhamnetin: yellow solid.; ^1H NMR (400 MHz, DMSO-*d*6) δ : 7.73 (d, J = 2Hz, 1H), 7.67 (dd, J = 8.2, 2.2 Hz, 1H), 6.93 (d, J = 8.2 Hz, 1H), 6.46 (d, J = 2.2 Hz, 1H), 6.18 (d, J = 2.2 Hz, 1H), 3.83 (s, 3H); ^{13}C NMR NMR (100 MHz, DMSO-*d*6) δ : 175.9, 164.0, 160.7, 156.2, 148.8, 147.4, 146.6, 135.8, 122.0, 121.7, 115.6, 111.7, 103.0, 98.2, 93.6, 55.8.

Azaleatin: yellow solid.; ^1H NMR (400 MHz, MeOD) δ = 7.70 (d, J = 2.8 Hz, 1H), 7.60 (dd, J = 8.8, 2.8 Hz, 1H), 6.87 (d, J = 2.2 Hz, 1H), 6.49 (d, J = 2.0 Hz, 1H), 6.38 (d, J =

2.0 Hz, 1H), 3.91 (s, 3H); ¹³C NMR NMR (100 MHz, MeOD) δ : 173.7, 164.7, 162.2, 160.1, 148.5, 146.3, 144.8, 138.7, 124.2, 121.3, 116.3, 115.7, 106.4, 96.8, 95.9, 56.5.

3-O-Methylquercetin: yellow solid.; ¹H NMR (400 MHz, MeOD) δ : 7.59 (d, *J* = 2.8 Hz, 1H), 7.50 (dd, *J* = 8.8, 2.8 Hz, 1H), 6.88 (d, *J* = 8.8 Hz, 1H), 6.35 (d, *J* = 2.0 Hz, 1H), 6.16 (d, *J* = 2.0 Hz, 1H), 3.76 (s, 3H); ¹³C NMR NMR (100 MHz, MeOD) δ : 178.7, 164.5, 161.8, 157.1, 156.7, 148.6, 145.2, 138.2, 121.7, 121.0, 115.2, 115.1, 104.6, 98.5, 93.4, 59.2.

Tamarixetin: yellow solid.; ¹H NMR (400 MHz, MeOD) δ : 7.76-7.73 (m, 2H), 7.05 (d, *J* = 8.8 Hz, 1H), 6.39 (d, *J* = 2.4 Hz, 1H), 6.18 (d, *J* = 2.4 Hz, 1H), 3.93 (s, 3H).

Rhamnetin: yellow solid.; ¹H NMR (400 MHz, MeOD) δ : 7.76 (d, *J* = 2.4 Hz, 1H), 7.66 (dd, *J* = 8.8, 2.0 Hz, 1H), 6.88 (d, *J* = 8.8 Hz, 1H), 6.58 (d, *J* = 2.4 Hz, 1H), 6.31 (d, *J* = 2.4 Hz, 1H), 3.89 (s, 3H).

- iii. MTT solution for the final concentration of 0.5 mg/ml was added to the culture medium and incubated for 6 hours. After discarding the medium formazan crystals were dissolved in 10% sodium dodecyl sulfate (SDS) solution for overnight incubation. Absorbance at 570 nm was measured using microplate reader, and the cell proliferation rate was calculated by the formula: Cell proliferation (%) = [(mean OD value of treated well – mean OD value of the blank) × 100%] / (mean OD value of untreated well – mean OD value of the blank). The experiment with six repeats in each concentration was replicated at least independent three times.
- iv. Cells were incubated overnight to allow cells to attach the surface. Subsequently cells

were induced with 2 ng/ml of TGF β with or without derivatives. After 24 hours, cells were washed twice with cold phosphate buffered saline (PBS) and fixed with 3.7% paraformaldehyde for 20 minutes at room temperature followed by rehydration with PBS and incubated in blocking solution containing 1% bovine serum albumin (BSA) and 0.1% Tween20 for 2 hours. The slides were incubated with the primary antibody anti-collagen I at 1/100 dilution and anti- α SMA at 1/100 dilution for overnight at 4 °C. Consequently, the slides were incubated for 1 hour with secondary antibody at 1/250 dilution after washing with PBS three times. The slides were mounted using ProLong Diamond with DAPI and observed under a Leica TCS SP8 confocal microscope for imaging.

Acknowledgments

This thesis is dedicated to my beloved parents and brother, my father Ganbold, my mother Buyandelger and my brother Munkhtuvshin, who had to overcome my mom's tough disease alone while I was writing my dissertation over the course of these last years but have never forgotten any single moment to encourage me and give me a reason to accomplish my thesis.

Most of all, my sincere appreciation and acknowledgment to my thesis supervisor, professor Hiroko Isoda, Ph.D, for her competent guidance and patience. Without her useful critiques, and scientific encouragements this thesis work would not have been possible.

I would also like to extend my sincere gratitude to my co-supervisors, professor Nobuhiro Ohkohchi, MD, Ph.D who supervised me during my first year for his valuable advices on the research topic from clinical point of view; professor Yun Wen Zheng, Ph.D for tirelessly supporting me and stimulating my scientific reasoning, and for his scientific advices; Yusaku Miyamae, Ph.D for sharing his competent and ever-useful advices in daily experiments, his regular discussions with guidance, and his kindness. I would also like to thank my colleague and team leader, Farhana Ferdousi, Ph.D, for initiating me in statistics, and sharing me her extensive experiences in the scientific publication procedure.

Special thanks to professor Tominaga, Ph.D, and Yasuhiro Shimamoto, Ph.D; for their technical support by providing compounds; Yohei Owada, MD, PhD; Yusuke Ozawa, MD, Ph.D, assistant Aoki Takahashi for their incredible support in mice experiments; and to all of my professors, colleagues, and friends of Isoda lab for their daily assistance, interesting talks, and encouragement for the completion of this work.

This work was partially supported by the JST-JICA - Japan Science and Technology Agency and the Japan International Cooperation Agency (SATREPS), and JST-Center of Innovation (COI) project; and MJEED - Mongolian-Japan Engineering Education Development Project.

References

1. Yang, J.H.; Shin, B.Y.; Han, J.Y.; Kim, M.G.; Wi, J.E.; Kim, Y.W.; Cho, I.J.; Kim, S.C.; Shin, S.M.; Ki, S.H. Isorhamnetin protects against oxidative stress by activating Nrf2 and inducing the expression of its target genes. *Toxicol. Appl. Pharmacol.* **2014**, *274*, 293–301.
2. Hu, S.; Huang, L.; Meng, L.; Sun, H.; Zhang, W.; Xu, Y. Isorhamnetin inhibits cell proliferation and induces apoptosis in breast cancer via Akt and mitogen-activated protein kinase signaling pathways. *Mol. Med. Rep.* **2015**, *12*, 6745–6751.
3. Lee, H.J.; Lee, H.J.; Lee, E.O.; Ko, S.G.; Bae, H.S.; Kim, C.H.; Ahn, K.S.; Lu, J.; Kim, S.H. Mitochondria-cytochrome C-caspase-9 cascade mediates isorhamnetin-induced apoptosis. *Cancer Lett.* **2008**, *270*, 342–353.
4. Dou, W.; Zhang, J.; Li, H.; Kortagere, S.; Sun, K.; Ding, L.; Ren, G.; Wang, Z.; Mani, S. Plant flavonol isorhamnetin attenuates chemically induced inflammatory bowel disease via a PXR-dependent pathway. *J. Nutr. Biochem.* **2014**, *25*, 923–933.
5. Lee, J.; Jung, E.; Lee, J.; Kim, S.; Huh, S.; Kim, Y.; Kim, Y.; Byun, S.Y.; Kim, Y.S.; Park, D. Isorhamnetin represses adipogenesis in 3T3-L1 cells. *Obes. (Silver Spring)* **2009**, *17*, 226–232.
6. Zar Kalai, F.; Han, J.; Ksouri, R.; Abdelly, C.; Isoda, H. Oral administration of *Nitraria retusa* ethanolic extract enhances hepatic lipid metabolism in db/db mice model “BKS.Cg-Dock7m^{+/+} Leprdb/J” through the modulation of lipogenesis-lipolysis balance. *Food Chem. Toxicol.* **2014**, *72*, 247–256.

7. Zar Kalai, F.; Han, J.; Ksouri, R.; El Omri, A.; Abdelly, C.; Isoda, H. Antiobesity effects of an edible halophyte *Nitraria retusa* Forssk in 3T3-L1 preadipocyte differentiation and in C57B6J/L mice fed a high fat diet-induced obesity. *Evidence-based Complement. Altern. Med.* **2013**, *2013*, 368658.
8. Wu, L.; Zhang, Q.; Mo, W.; Feng, J.; Li, S.; Li, J.; Liu, T.; Xu, S.; Wang, W.; Lu, X.; et al. Quercetin prevents hepatic fibrosis by inhibiting hepatic stellate cell activation and reducing autophagy via the TGF- β 1/Smads and PI3K/Akt pathways. *Sci. Rep.* **2017**, *7*, 9289.
9. Marcolin, É.; Forgiarini, L.F.; Rodrigues, G.; Tieppo, J.; Borghetti, G.S.; Bassani, V.L.; Picada, J.N.; Marroni, N.P. Quercetin Decreases Liver Damage in Mice with Non-Alcoholic Steatohepatitis. *Basic Clin. Pharmacol. Toxicol.* **2013**, *112*, 385–391.
10. Li, G.; Zeng, X.; Xie, Y.; Cai, Z.; Moore, J.C.; Yuan, X.; Cheng, Z.; Ji, G. Pharmacokinetic properties of isorhamnetin, kaempferol and quercetin after oral gavage of total flavones of *Hippophae rhamnoides* L. in rats using a UPLC-MS method. *Fitoterapia* **2012**, *83*, 182–191.
11. Leclercq, I.A.; Lebrun, V.A.; Stärkel, P.; Horsmans, Y.J. Intrahepatic insulin resistance in a murine model of steatohepatitis: Effect of PPAR γ agonist pioglitazone. *Lab. Investig.* **2007**, *87*, 56–65.
12. Owada, Y.; Tamura, T.; Tanoi, T.; Ozawa, Y.; Shimizu, Y.; Hisakura, K.; Matsuzaka, T.; Shimano, H.; Nakano, N.; Sakashita, S.; et al. Novel non-alcoholic

- steatohepatitis model with histopathological and insulin-resistant features. *Pathol. Int.* **2018**, *68*, 12–22.
13. Younossi, Z.M.; Koenig, A.B.; Abdelatif, D.; Fazel, Y.; Henry, L.; Wymer, M. Global epidemiology of nonalcoholic fatty liver disease—Meta-analytic assessment of prevalence, incidence, and outcomes. *Hepatology* **2016**, *64*, 73–84.
 14. Donnelly, K.L.; Smith, C.I.; Schwarzenberg, S.J.; Jessurun, J.; Boldt, M.D.; Parks, E.J. Sources of fatty acids stored in liver and secreted via lipoproteins in patients with nonalcoholic fatty liver disease. *J. Clin. Invest.* **2005**, *115*, 1343–1351.
 15. Diraison, F.; Moulin, P.; Beylot, M. Contribution of hepatic de novo lipogenesis and reesterification of plasma non esterified fatty acids to plasma triglyceride synthesis during non-alcoholic fatty liver disease. *Diabetes Metab.* **2003**, *29*, 478–485.
 16. Ameer, F.; Scanduzzi, L.; Hasnain, S.; Kalbacher, H.; Zaidi, N. De novo lipogenesis in health and disease. *Metabolism* **2014**, *63*, 895–902.
 17. Lambert, J.E.; Roman, M.A.R.; Browning, J.D.; Parks, E.J. Increased De Novo Lipogenesis Is a Distinct Characteristic of Individuals With Nonalcoholic Fatty Liver Disease. *Gastroenterology* **2014**, *146*, 726–735.
 18. Kato, K.; Ninomiya, M.; Tanaka, K.; Koketsu, M. Effects of Functional Groups and Sugar Composition of Quercetin Derivatives on Their Radical Scavenging Properties. *J. Nat. Prod.* **2016**, *79*, 1808–1814.
 19. Horton, J.D.; Goldstein, J.L.; Brown, M.S. SREBPs: activators of the complete

- program of cholesterol and fatty acid synthesis in the liver. *J. Clin. Invest.* **2002**, *109*, 1125–1131.
20. Charlton, M.; Sreekumar, R.; Rasmussen, D.; Lindor, K.; Nair, K.S. Apolipoprotein synthesis in nonalcoholic steatohepatitis. *Hepatology* **2002**, *35*, 898–904.
 21. Yin, C.; Evason, K.J.; Asahina, K.; Stainier, D.Y.R. Hepatic stellate cells in liver development, regeneration, and cancer. *J. Clin. Invest.* **2013**, *123*, 1902–1910.
 22. Bian, Z.; Ma, X. Liver fibrogenesis in non-alcoholic steatohepatitis. *Front. Physiol.* **2012**, *3 JUL*, 1–7.
 23. Yang, J.H.; Kim, S.C.; Kim, K.M.; Jang, C.H.; Cho, S.S.; Kim, S.J.; Ku, S.K.; Cho, I.J.; Ki, S.H. Isorhamnetin attenuates liver fibrosis by inhibiting TGF- β /Smad signaling and relieving oxidative stress. *Eur. J. Pharmacol.* **2016**, *783*, 92–102.
 24. Dooley, S.; Ten Dijke, P. TGF- β in progression of liver disease. *Cell Tissue Res.* **2012**, *347*, 245–256.
 25. Yang, L.; Roh, Y.S.; Song, J.; Zhang, B.; Liu, C.; Loomba, R.; Seki, E. TGF- β signaling in hepatocytes participates in steatohepatitis through regulation of cell death and lipid metabolism. *Hepatology* **2014**, *59*, 483–495.
 26. Chakraborty, J.B.; Oakley, F.; Walsh, M.J. Mechanisms and Biomarkers of Apoptosis in Liver Disease and Fibrosis. *Int. J. Hepatol.* **2012**, *2012*, 1–10.
 27. Feldstein, A.E.; Canbay, A.; Angulo, P.; Taniai, M.; Burgart, L.J.; Lindor, K.D.; Gores, G.J. Hepatocyte apoptosis and Fas expression are prominent features of

- human nonalcoholic steatohepatitis. *Gastroenterology* **2003**, *125*, 437–443.
28. Chen, Z.; Yu, R.; Xiong, Y.; Du, F.; Zhu, S. A vicious circle between insulin resistance and inflammation in nonalcoholic fatty liver disease. *Lipids Health Dis.* **2017**, *16*, 1–9.
 29. Manach, C.; Scalbert, A.; Morand, C.; Rémésy, C.; Jiménez, L. Polyphenols : food sources and bioavailability. *Am. J. Clin. Nutr.* **2004**, *79*, 727–747.
 30. Manach, C.; Williamson, G.; Morand, C.; Scalbert, A.; Rémésy, C. Bioavailability and bioefficacy of polyphenols in humans. I. Review of 97 bioavailability studies. *Am. J. Clin. Nutr.* **2005**, *81*, 230S-242S.
 31. Spencer, J.P.E.; Abd El Mohsen, M.M.; Rice-Evans, C. Cellular uptake and metabolism of flavonoids and their metabolites: Implications for their bioactivity. *Arch. Biochem. Biophys.* **2004**, *423*, 148–161.
 32. Koirala, N.; Thuan, N.H.; Ghimire, G.P.; Thang, D. Van; Sohng, J.K. Methylation of flavonoids: Chemical structures, bioactivities, progress and perspectives for biotechnological production. *Enzyme Microb. Technol.* **2016**, *86*, 103–116.
 33. Spencer, J.P.E.; Kuhnle, G.G.C.; Williams, R.J.; Rice-Evans, C. Intracellular metabolism and bioactivity of quercetin and its in vivo metabolites. *Biochem. J.* **2003**, *372*, 173–181.
 34. Higashi, T.; Friedman, S.L.; Hoshida, Y. Hepatic stellate cells as key target in liver fibrosis. *Adv. Drug Deliv. Rev.* **2017**, *121*, 27–42.
 35. Puche, J.E.; Saiman, Y.; Friedman, S.L. Hepatic stellate cells and liver fibrosis.

- Compr. Physiol.* **2013**, *3*, 1473–1492.
36. Zhang, C.Y.; Yuan, W.G.; He, P.; Lei, J.H.; Wang, C.X. Liver fibrosis and hepatic stellate cells: Etiology, pathological hallmarks and therapeutic targets. *World J. Gastroenterol.* **2016**, *22*, 10512–10522.
37. Ganbold, M.; Shimamoto, Y.; Ferdousi, F.; Tominaga, K.; Isoda, H. Antifibrotic effect of methylated quercetin derivatives on TGF β -induced hepatic stellate cells. *Biochem. Biophys. Reports* **2019**, *20*, 100678.
38. Shi, Z.H.; Li, N.G.; Tang, Y.P.; Wei-Li; Lian-Yin; Yang, J.P.; Hao-Tang; Duan, J.A. Metabolism-based synthesis, biologic evaluation and SARs analysis of O-methylated analogs of quercetin as thrombin inhibitors. *Eur. J. Med. Chem.* **2012**, *54*, 210–222.
39. Parveen, S.; Riaz, N.; Saleem, M.; Khan, J.; Ahmad, S.; Ashraf, M.; Ejaz, S.A.; Tareen, R.B.; Jabbar, A. Bioactive phenolics from launaea intybacea. *J. Chem. Soc. Pakistan* **2012**, *34*, 1513–1519.
40. Villaume, S.A.; Fu, J.; N'Go, I.; Liang, H.; Lou, H.; Kremer, L.; Pan, W.; Vincent, S.P. Natural and Synthetic Flavonoids as Potent Mycobacterium tuberculosis UGM Inhibitors. *Chem. - A Eur. J.* **2017**, *23*, 10423–10429.
41. Yamauchi, K.; Mitsunaga, T.; Inagaki, M.; Suzuki, T. Synthesized quercetin derivatives stimulate melanogenesis in B16 melanoma cells by influencing the expression of melanin biosynthesis proteins MITF and p38 MAPK. *Bioorganic Med. Chem.* **2014**, *22*, 3331–3340.

42. Guzmán-Gutiérrez, S.L.; Nieto-Camacho, A.; Castillo-Arellano, J.I.; Huerta-Salazar, E.; Hernández-Pasteur, G.; Silva-Miranda, M.; Ello-Nájera, O.A.; Sepúlveda-Robles, O.; Espitia, C.I.; Reyes-Chilpa, R. Mexican propolis: A source of antioxidants and anti-inflammatory compounds, and isolation of a novel chalcone and ϵ -caprolactone derivative. *Molecules* **2018**, *23*, E334.
43. Akhurst, R.J.; Hata, A. Targeting the TGF β signalling pathway in disease. *Nat. Rev. Drug Discov.* **2012**, *11*, 790–811.
44. Gressner, A.M.; Weiskirchen, R.; Breitkopf, K.; Dooley, S. Roles of TGF-beta in hepatic fibrosis. *Clin. Chem.* **2002**, *7*, d793-807.
45. Piersma, B.; Bank, R.A.; Boersema, M. Signaling in Fibrosis: TGF- β , WNT, and YAP/TAZ Converge. *Front. Med.* **2015**, *2*, 1–14.
46. Xu, F.; Zhou, D.; Meng, X.; Wang, X.; Liu, C.; Huang, C.; Li, J.; Zhang, L. Smad2 increases the apoptosis of activated human hepatic stellate cells induced by TRAIL. *Int. Immunopharmacol.* **2016**, *32*, 76–86.
47. Ezhilarasan, D.; Sokal, E.; Najimi, M. Hepatic fibrosis: It is time to go with hepatic stellate cell-specific therapeutic targets. *Hepatobiliary Pancreat. Dis. Int.* **2018**, *17*, 192–197.
48. Fabregat, I.; Moreno-Càceres, J.; Sánchez, A.; Dooley, S.; Dewidar, B.; Giannelli, G.; ten Dijke, P. TGF- β signalling and liver disease. *FEBS J.* **2016**, *283*, 2219–2232.
49. Kawada, N.; Seki, S.; Inoue, M.; Kuroki, T. Effect of antioxidants, resveratrol,

- quercetin, and N-acetylcysteine, on the functions of cultured rat hepatic stellate cells and kupffer cells. *Hepatology* **1998**, *27*, 1265–1274.
50. Jadeja, R.; Devkar, R. V; Nammi, S.; Jadeja, R.; Devkar, R. V.; Nammi, S. Herbal medicines for the treatment of nonalcoholic steatohepatitis: current scenario and future prospects. *Evid. Based. Complement. Alternat. Med.* **2014**, *2014*, 648308.
 51. Li, Q.; Ren, F.Q.; Yang, C.L.; Zhou, L.M.; Liu, Y.Y.; Xiao, J.; Zhu, L.; Wang, Z.G. Anti-proliferation Effects of Isorhamnetin on Lung Cancer Cells in Vitro and in Vivo. *Asian Pac J Cancer Prev* **2015**, *16*, 3035–3042.
 52. Hernández-Aquino, E.; Muriel, P. Beneficial effects of naringenin in liver diseases: Molecular mechanisms. *World J. Gastroenterol.* **2018**, *24*, 1679–1707.
 53. Reccia, I.; Kumar, J.; Akladios, C.; Viridis, F.; Pai, M.; Habib, N.; Spalding, D. Non-alcoholic Fatty Liver Disease: A sign of systemic disease. *Metabolism.* **2017**, *72*, 94–108.
 54. Ferré, P.; Foufelle, F. Hepatic steatosis: A role for de novo lipogenesis and the transcription factor SREBP-1c. *Diabetes, Obes. Metab.* **2010**.
 55. Brunt, E.M.; Kleiner, D.E.; Wilson, L.A.; Belt, P.; Brent, A.; Neuschwander-Tetri The NAS and the Histopathologic Diagnosis of NAFLD: Distinct Clinicopathologic Meanings. *Hepatology* **2011**, *53*, 810–820.
 56. Yokozawa, T.; Kim, H.Y.; Cho, E.J.; Choi, J.S.; Chung, H.Y. Antioxidant effects of isorhamnetin 3,7-di-O-β-D-glucopyranoside isolated from mustard leaf (*Brassica juncea*) in rats with streptozotocin-induced diabetes. *J. Agric. Food*

Chem. **2002**, *50*, 5490–5495.

57. Lee, U.E.; Friedman, S.L. Mechanisms of Hepatic Fibrogenesis. *Best Pract. Res. Clin. Gastroenterol.* **2011**, *25*, 195–206.
58. Zhang, Y.; Gu, M.; Cai, W.; Yu, L.; Feng, L.; Zhang, L.; Zang, Q.; Wang, Y.; Wang, D.; Chen, H.; et al. Dietary component isorhamnetin is a PPAR γ antagonist and ameliorates metabolic disorders induced by diet or leptin deficiency. *Sci. Rep.* **2016**, *6*, 19288.